Title

Development of a Portable Chemical Detection Platform

Author

Fung, Stephanie

Publication Date

2023

Peer reviewed|Thesis/dissertation

Development of a Portable Chemical Detection Platform

By

STEPHANIE FUNG
DISSERTATION

Submitted in partial satisfaction of the requirements for the degree of

DOCTOR OF PHILOSOPHY

in

Mechanical and Aerospace Engineering

in the

OFFICE OF GRADUATE STUDIES

of the

UNIVERSITY OF CALIFORNIA

DAVIS

Approved:

Cristina Davis, Chair

Nicholas Kenyon

Erkin Seker

Committee in Charge

2023

Stephanie Fung
November 2023
Mechanical and Aerospace Engineering

Development of a Portable Chemical Detection Platform

Abstract

Trace chemical detection plays an important role in evaluating environmental hazards as well as benign chemical sources. The adequate odorization of natural gas is critical to identify gas leaks and to reduce accidents. To ensure odorization, natural gas utility companies collect samples to be processed at core facilities or a trained human technician smells a diluted natural gas sample. In this dissertation, a low power dual-polarity ionization-based detector was developed. The detector electronics are operated with a single 9 V battery and provide concentration sensitive voltage outputs. The complete assembly and operation of the detector is detailed. The detector can achieve a system step response of ~1.6 s. We performed laboratory measurements with several ionized chemicals using both positive and negative mode. The results showed highly linear responses at trace concentrations as low as 100 ppb. Following, we report a detection platform that addresses the lack of mobile solutions capable of providing quantitative analysis of mercaptans, a class of compounds used to odorize natural gas. Designed to be portable, the platform hardware facilitates extraction of mercaptans from natural gas, separation of individual mercaptan species, and quantification of odorant concentration, with results reported at point-of-sampling. The software was developed to accommodate skilled users as well as minimally trained operators. Detection and quantification of six commonly used mercaptan compounds at typical odorizing concentrations of 0.1–5 ppm was performed using the device. We demonstrate the potential of this technology to ensure natural gas odorizing concentrations throughout the distribution pipeline.

Acknowledgments

With my PhD journey coming to an end, I would like to thank the many people who have supported me through the long and winding road of graduate school.

The successful completion of this journey would truly not have been possible without my partner, Brandon Schlinker. I would have thrown in the towel and called it quits on the PhD many times if not for his unwavering belief in me. He has supported me in countless ways. At times, I wasn't sure if I had what it took to complete this, but he always knew that I did.

I would like to thank Cristina Davis, who as my major professor provided the resources pivotal to my development as an independent researcher. My time spent as a member of her BioMEMS lab has been nothing short of a once in a lifetime experience.

I would like to thank the members of my qualifying exam and dissertation committee for their valuable advice and guidance: Barbara Linke, Erkin Seker, Nesrin Sarigul-Klijn, Nick Kenyon and Vinod Narayanan.

I would like to thank all the BioMEMS lab members current and past who I have had the pleasure of working with however long or short that time may have been. I am forever grateful for Pat Gibson and Mitch McCartney, who provided me invaluable guidance and support especially leading up to the finish line. Much of this journey was quite a slog; I would not have made it without some amazing labmates. Special thanks to Alex Schmidt, Brad Chew, Dylan Koch, Michael LeVasseur, Nhi Trinh, Raquel Contreras, and Zander Fung for providing much needed graduate student banter from communal commiseration to belly busting laughs. I would also like to thank the three incredible post-docs I worked with: Eva Borras, Mei Yamaguchi, and Yasas Rajapakse.

I cannot thank each of them enough for their friendship, insights, and encouragements: they were beacons of shining hope and helped navigate me through the dimly lit parts of the path.

I very much appreciate my two cats: Mr. Frenchums and Oliver. My two furry dependents alleviated the feelings of loneliness that often accompanied being a doctoral student. Finally, I would not be here without the support of my family, especially my younger sister Lianna Fung. We are both the first in our family to attain doctoral degrees. She got there first, but I get the final words, thank you.

Declaration of Co-Authorship and Previous Publication

I hereby declare that this dissertation incorporates material that are the result of previous research conducted under the guidance and collaboration of Dr. Cristina Davis. I declare that this dissertation includes works that have been previously published/under publication review/will be submitted for publication in a peer reviewed journal, and that the published journal and/or conference proceedings are the original source.

Table of Contents

List of Figures

List of Tables

List of Acronyms

AC	Alternating Current
ADC	Analog to Digital Converter
ASTM	American Society for Testing and Materials
DC	Direct Current
DMS	Dimethyl Sulfide
EMI	Electromagnetic Interference
ETM	Ethyl Mercaptan
GC	Gas Chromatography
GUI	Graphical User Interface
IC	Integrated Circuit
IMS	Ion Mobility Spectrometry
IPM	iso-propyl Mercaptan
LTM	Low Thermal Mass
NPM	n-propyl Mercaptan
PCB	Printed Circuit Board
PID	Proportional, Integral, Derivative
PWM	Pulse Width Modulation
RF	Radio Frequency
RT	Retention Time
RTD	Resistance Temperature Detector
TBM	tert-butyl Mercaptan
THT	Tetrahydrothiophene
UV	Ultraviolet
VOC	Volatile Organic Compound

Chapter 1: Introduction

1.1 Need for Trace Chemical Detection

Trace chemical detection plays an important role in evaluating many types of environmental hazards as well as benign chemical sources. Volatile organic compounds (VOCs) in the air come from a variety of sources ranging from transportation emissions [1] to personal home care products [2], [3]. In addition, toxic industrial chemicals and materials have widespread use in societies and are agents that may cause harm to humans when exposures occur [4]. Monitoring is critical to ensure chemical concentrations do not exceed ambient exposure thresholds set by the Environmental Protection Agency (EPA) in the United States. Advances in monitoring technologies are needed to detect and quantify potentially harmful trace levels of these chemicals. In addition to detecting potentially harmful chemicals, there are many biogenic VOCs of interest that present interesting detection applications such as non-invasive agriculture disease detection [5]–[10] and biogenic breath VOCs for health monitoring [5], [11]–[13].

Traditionally, trace chemical detection in liquids and gasses is limited to laboratory environments. However, there are potential applications where chemical detection in a field portable form factor would be advantageous [14]. For example, on-site screening for chemicals in emergency response scenarios could help emergency responders [15], and real-time industrial process monitoring in manufacturing environments could help ensure worker safety [16]. Current instrumentation for chemical detection frequently requires AC power along with additional computing infrastructure and a laboratory environment. This does not lend itself to remote sensing applications in varying locations or harsh environments. Currently for gold standard measurements, environmental samples are captured, stored, and transported back to the laboratory to perform detection and analysis. Previous works have demonstrated that it is possible

to take commercially available parts and integrate them into a modular and reconfigurable system to measure volatile organic compounds (VOCs) [17], [18].

However, while there has been much work in preconcentration of samples to boost detection quantification ranges [19]–[22], robust portable chemical detectors are still needed to unlock advanced applications of chromatography in field applications [23]–[25].

1.2 Ion Detection

Several analytical techniques can be used to detect ions from gas phase trace levels of chemicals [25]–[28]. Regardless of the instrumentation, ionizing the sample and detecting the ion abundance are key to gauging ambient chemicals and VOCs concentration levels. There are several distinct ion source types, each with their own advantages and disadvantages [29]. Radioactive ion sources have been historically common in commercial devices based on the high energy ionization potential without the need for an external power source, but their application is discouraged based on legal and procedural ramifications [30], [31]. There are several developed methods (e.g., electrospray, corona discharge) that can provide non-radioactive ionization, but typically require high electric fields (>10 keV) and the external generation can prove to be an operational challenge for implementation in a mobile device. Photoionization, specifically UV lamp, is the ion source utilized for the work in this dissertation. The availability of commercially mature products is conducive to device integration. For example, a common UV lamp is filled with Krypton gas with a MgF_2 window providing a fixed ionization potential of 10.6 eV [32]. While the ionization energies achievable with UV lamps is much lower than the previously mentioned sources, this can add a dimension of selectivity to the overall detection device if the compounds of interest are within that ionization energy range.

There are two main types of detectors: direct measurement and multipliers. Direct measurement involves detection of the charge arriving at the detector while multipliers use electron multiplication [33]. While multiplier type detectors are capable of single ion detection and are widely implemented on commercial devices, direct measurement detectors are more amenable to portable device integration due to physical architecture and significantly lower voltage requirements. For example, the electron multiplier detector on a contemporary gas chromatography-mass spectrometry (GC-MS) system uses applied voltages of up to 3 kV [34]. Direct measurement detectors, namely plate detectors, can be designed such that no applied

voltage is required, or the voltage can be on the order of volts scaling with the dimensions of the detector.

Additionally, there is the polarity of the ion species to consider. Gas phase chemicals subject to an ionization source can generate both positive and negative ions. Detection of ions of both polarities is important in the application of hazardous trace chemical detection. Hazardous VOCs typically generate positive ions by different mechanisms at the ionization source such as loss of electrons or by adduct ion formation and must be detected by negatively biased detector [35]. In contrast, hazardous ordnance related compounds such as explosives can be only detected as negative ions with few exceptions. Sensing these compounds is achieved with aid of a dopant and making stable adduct ions such as chloride adducts. The resulting ions can survive several milliseconds in air at ambient pressure before being neutralized due to collisions. Significant changes in circuitry are required when attempting to detect negative ions with an electron multiplier detector to decouple the high voltage bias [36]. Conversely, direct measurement detectors can readily detect positive and negative ions. It is necessary to have detection technologies that can match these timescales and amplify the low ion currents of both polarities to detect chemicals of interest. In this dissertation, a microfabricated direct measurement plate detector is developed to employ the advantages offered by this detector type.

The general schema of electronic detection of chemical ions with a plate detector is illustrated in **Figure 1**. A flow of inert gas is utilized as a carrier to transport the ionized sample to a conducting electrode. As the ions are neutralized on the electrode, a current is induced proportional to the concentration of the ion abundance. Sensing trace chemicals <1 ppm results in current levels in

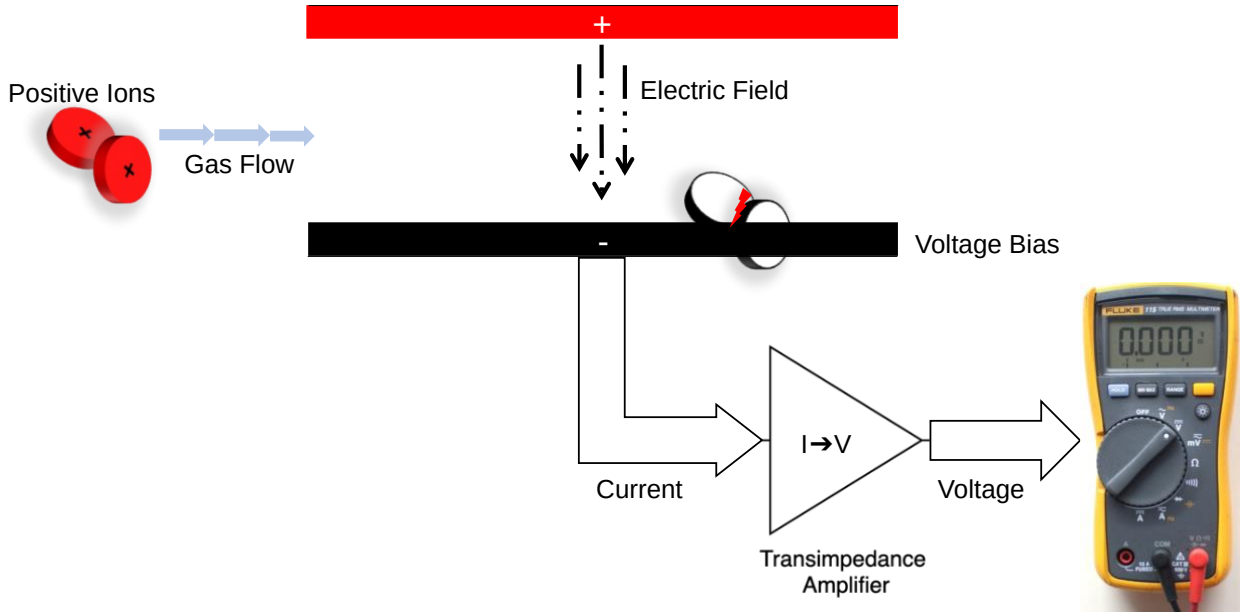

Figure 1. Ion detection process.
Ions are carried by an inert gas to an electrode charged with opposite polarity and a current is induced proportional to the abundance of the ion concentration. The current is then amplified and converted to a voltage for readout.

the picoampere range, and the design of the fixturing and electronics to successfully detect such low levels is non-trivial. Furthermore, for low power mobile operation, it is important to consider performance metrics when operated with a battery such as output stability, expected total run-time, and bias configuration. For instance, previously reported detector electronics claimed low power battery operation [37], but do not disclose such battery-operated performance metrics. Many miniaturized trace chemical detectors have been developed in the recent decades [27], [38]–[41]. However, these works rely on benchtop commercial readout devices unsuitable for mobile application.

Previous works have reported ionization methods and detection electronics in a piecemeal and ad hoc fashion. Few references provide the details needed to fully replicate the detection

apparatus. No study had been reported for a battery powered ion detection system with the capability to detect ions in both positive and negative modes.

1.3 Sensing Adequate Odorization of Natural Gas

Natural gas is a major energy source in the U.S. making up 32% of the primary energy consumption [42]. Due to the potential dangers involved with natural gas leaks, there are federal regulations (49 CFR 192.625) in place that provision for the odorization of distribution-grade natural gas to a detectable concentration in air at one-fifth the lower explosive limit (LEL) such that humans would be able to detect a potential gas leak with a normal sense of smell [43]. Additionally, natural gas is largely comprised of CH_4, which has climate change impact potential that is 25 times greater than CO_2 [44]. The adequate odorization of natural gas is critical for the identification of gas leaks ensuring both the safe supply of this widely used energy source and the prevention of greenhouse gas leakage. Sulfur containing odorant compounds [e.g., mercaptan compounds, tetrahydrothiophene (THT) and dimethyl sulfide (DMS)] are injected by pipeline operators and gas distribution companies to effectively odorize the gas [45].

It is critical to test distribution lines at varying points, as odorant concentrations can decrease due to oxidation of rusting pipes, adsorption onto pipes or appliances, and absorption into liquids [46]. Some gas distribution entities monitor the composition at waypoint stations that are midstream, but this does not guarantee the sufficient odorization of gas at points further downstream. Operators may opt to collect a sample of natural gas to test with standard analytical laboratory methods. These samples need to be analyzed within a certain time based on the sampling vessel used [47] and need to be sent to an outside lab if the gas distribution entity does not have in-house analytical capabilities. Additionally, standard analyses often only provide “total sulfur” readings. Such readings are inflated by the presence of sulfur compound impurities [48] found in natural gas lines, rather than providing individual concentrations of the added odorants.

Alternatively, pipeline operators may employ an ASTM standard (ASTM D6273 – 08) that outlines test methods for natural gas odor intensity. This method depends on the human sense of smell

as the procedures call for a trained person to “sniff at the apparatus exhaust” to gauge odorization. However, odor thresholds vary from person to person [49], and this method is subject to biological factors such as odor fatigue or loss of smell. There are conditions that may result in olfactory impairment whether it is due to a condition or illness such as COVID-19 [50]. Overall, this industry sector needs a portable, robust, and repeatable mechanism for in-field monitoring of odorant compound levels throughout all points of distribution.

1.4 Research Objectives

The goal of this work is to realize sampling, pre-concentration, separation, and detection of odorant compounds in natural gas integrated into a device suited for field use. The work is comprised of the following objectives as laid out in the subsequent chapters:

Objective: **Develop low power ion detector for trace level chemical sensing.** In Chapter 2, a dual-polarity portable ion detector powered from a standard 9 V battery is reported. The detector was designed to be compact and low power such that it could be integrated into a mobile chemical sensing platform while providing performance that matches or exceeds that of a gold-standard benchtop instrument.

Objective: **Integrate a proof-of-concept device for monitoring odorant compounds in natural gas and characterize the performance of the device in the field.** In Chapter 3, a new platform is presented with hardware and software specifically designed and tailored to target natural gas odorant detection. The resulting device is the first of its kind, providing sample-to-analysis odorant concentration monitoring suitable for mobile deployment. Experimental measurements demonstrate speciation of targeted odorant compounds.

Chapter 2: Battery powered dual-polarity ion detector for trace chemical sensing

Trace chemical detection plays an important role in evaluating environmental hazards as well as benign chemical sources. In this chapter, the development of a low power dual-polarity ionization-based detector is detailed. The detector electronics are operated with a single 9 V battery and provide an output voltage that varies depending on the concentration of the chemical measured. The detection mode can be set manually with the on-board electronics or can be controlled with a microcontroller compatible digital input. The complete assembly and operation of the detector is detailed. The features of the detector make it suitable to be operated as a standalone system or to be integrated as a sub-system into a field-portable analytical platform. The detector achieved a system step response of ~1.6 s. Laboratory measurements were performed with several ionized chemicals using both positive and negative mode. The results showed highly linear responses at trace concentrations as low as 100 ppb.

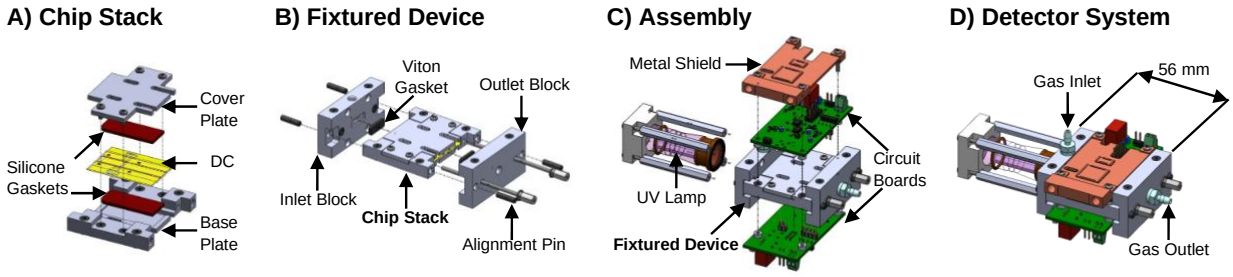

Figure 2. Chemical detection system

The chemical detection system is a combination of component modules that together allow for trace positive and negative charged ion detection. (A) The device is sandwiched in a stack held in place with two silicone gaskets compressed by metal cover and base plates. (B) The chip stack is clamped between two metal blocks with Viton gaskets at the inlet and outlet to create an airtight seal. (C) The circuit board electronics and the ionization source attach to the fixtured device and are interchangeable to meet application needs. (D) Fully assembled detector system.

The detector system is a combination of modules that together provide low power and trace detection of charged ion species for chemical sensing (**Figure 2**). The sensing component of the

system is a microfabricated device called μDC (microfabricated detector channel) that detects charged ions. This device is housed within a custom fixture which accommodates an ionization source and facilitates gas phase sample introduction. Custom control and signal conditioning electronics are packaged on printed circuit boards (PCBs). The system assembly measures 50 mm x 55 mm x 25 mm. The system is powered by a 9 V battery, thus making it suitable for field portable applications.

2.1 Microfabricated detector channel (µDC)

2.1.1 Device Fabrication

The µDC devices (**Figure 3**) were fabricated with the manufacturing method previously used by our group and reported on in [51]. The process steps were carried out in our campus Class 100 cleanroom facility (Center for Nano-MicroManufacturing, University of California Davis). The starting substrate was a 100 mm round, 700 µm thick borosilicate glass wafer (Borofloat 33; Schott North America, Inc., Louisville, KY).

An electron beam (CHA Industries AutoTech II, Fremont, CA) was used to deposit thin film layers of conductive Cr and Au having thickness of 20 and 100 nm respectively. Briefly, NR9-1500PY negative photoresist (Futurrex Inc., Franklin, NJ) was spun onto the wafer at 3000 rpm, and soft

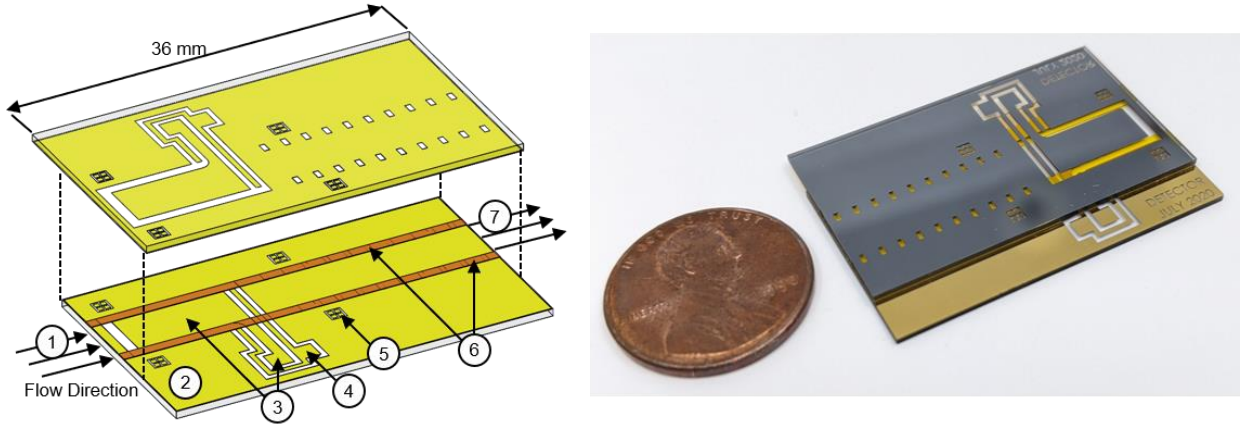

Figure 3. Microfabricated detector channel (µDC)
Microfabricated detector channel (µDC) is manufactured on a borosilicate substrate using standard photolithography and etch techniques. (1) Inlet to the device; (2) Patterned metal ground plane; (3) The detector electrode and trace leading out to the pad; (4) Bias voltage surrounds the detector electrode on the chip to guard against leakage current; (5) Alignment markers; (6) Polyimide spacers that define the channel dimensions; (7) The device outlet. A photograph of the assembled device is shown next to a US penny to provide scale.

baked at 150 ºC for 3.5 minutes. Photolithography was performed using a Karl-Suss M4A mask aligner with flood exposure at 15 mW/cm^2 for 24 seconds to define the electrodes using a full contact transparency mask (CAD/Art Services, Inc., Bandon, OR). A post-exposure bake of 100 ºC for 3.5 minutes was followed by development for 20 seconds in RD6 developer solution (Futurrex Inc., Franklin, NJ). A hard bake was then performed at 130 ºC for 3 minutes. The pattern was etched into the metal layers with a solution of diluted aqua regia (3:1:10 HCl:HNO_3:H_2O), followed by an etch in Cr etchant 1020 (Transene Company, Inc., Danvers, MA). Following removal of the photoresist in a sonicated solution of RR41 resist remover (Futurrex Inc., Franklin, NJ), dicing of the wafer created rectangular chip halves with symmetric electrodes.

The mask aligner and a programmable furnace (Naytech,Vulcan 3-550) were used to form the gas flow path of the µDC device. Placing a strip of laminated polyimide film, 500FN131 (Dupont, Wilmington, DE), between two previously patterned glass chips, a temporary bond was set with the mask aligner, matching the locations of the top and bottom detector electrodes. The device was then transferred to the programmable furnace where it was thermally bonded at 210 ºC for 15 minutes with an applied pressure of 5 psi.

2.1.2 Device Operation

The detector channel dimensions are defined with the fabrication process whereby the laminated film acts as a spacer and determines the height and width of the channel that is formed (**Figure 3**). The inlet and outlet to the µDC is the slit formed at each end of the bonded device. Ionized sample flows into the device at the inlet which is closest to the detector electrodes. The sample

continues through the channel to the outlet slit where it can be properly exhausted or continue to be analyzed by other methods.

At the device inlet, there are two detector electrodes, with dimensions 5.00 x 10.75 mm, patterned on each of the chip halves that run parallel to each other along the formed channel. The device dimensions are detailed in **Figure 4**. Each detector electrode is biased to either a positive or negative voltage. The function of the biased voltage is two-fold: first the biased voltage acts to attract the ion of the opposite charge to the sensing electrode, second the electrode directly opposite deflects the ions of the same charge to the appropriate sensing electrode. Ions neutralizing on the detection electrode generate a current proportional to the concentration of the ionized chemical in the sample. The bias electrode is set to the respective bias voltage and serves as an on-chip guard ring to minimize current leakage from the detector electrode. Patterned metal traces leading to metal pads on the device provide an electrical interface to the electrodes that are accessible through an opening in the fixture.

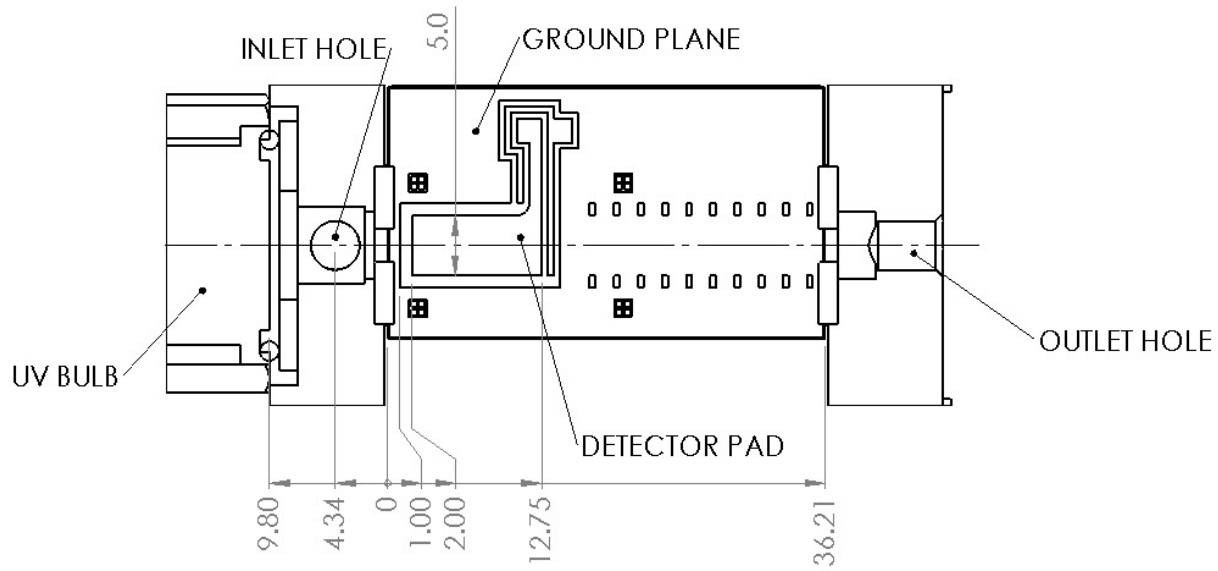

Figure 4. Detailed dimensions (in mm) of the fixtured µDC device

2.2 System Assembly

The µDC is housed in a metal fixture with the complete assembly process shown (**Figure 2**). The device is clamped tightly in place between two silicone gaskets in an aluminum housing, which provides electrical shielding and structural integrity. The flow paths into and out of the device are sealed with laser-cut Viton gaskets. These are mated with the aluminum inlet and outlet blocks and are aligned with precision stainless steel dowel pins and held with fasteners. The PCBs are designed such that spring metal pins contacts (Mill-Max, Oyster Bay, NY) fit precisely through slots in the metal fixture to make an electrical connection to the corresponding electrode pads on the device. Additionally, a copper shielding plate is mounted above the circuit boards to provide additional shielding. The ionization source is installed on the inlet block over the ionization chamber and sealed with a standard O-ring. Gas flow connections are made at the inlet and outlet via standard 10-32 thread fittings.

2.2.1 Sample Introduction and Ionization

The cross-section view shows the detail of the sample flow path through the assembled system (**Figure 5**). Sample is introduced into the inlet block which has machined 10-32 threads for using standard tube fitting adapters. A machined opening in the inlet block serves as an ionization chamber where the sample is ionized with a 10.6 eV Kr UV bulb (Analytical West, Corona, CA). Photoionization was utilized for the experiments carried out in this article, but it is possible to adapt this fixture for alternative ionization sources with higher energy potentials such as Ni-63

(radioactive), corona discharge, or other advanced ionization method. Directly following ionization, the sample enters the µDC.

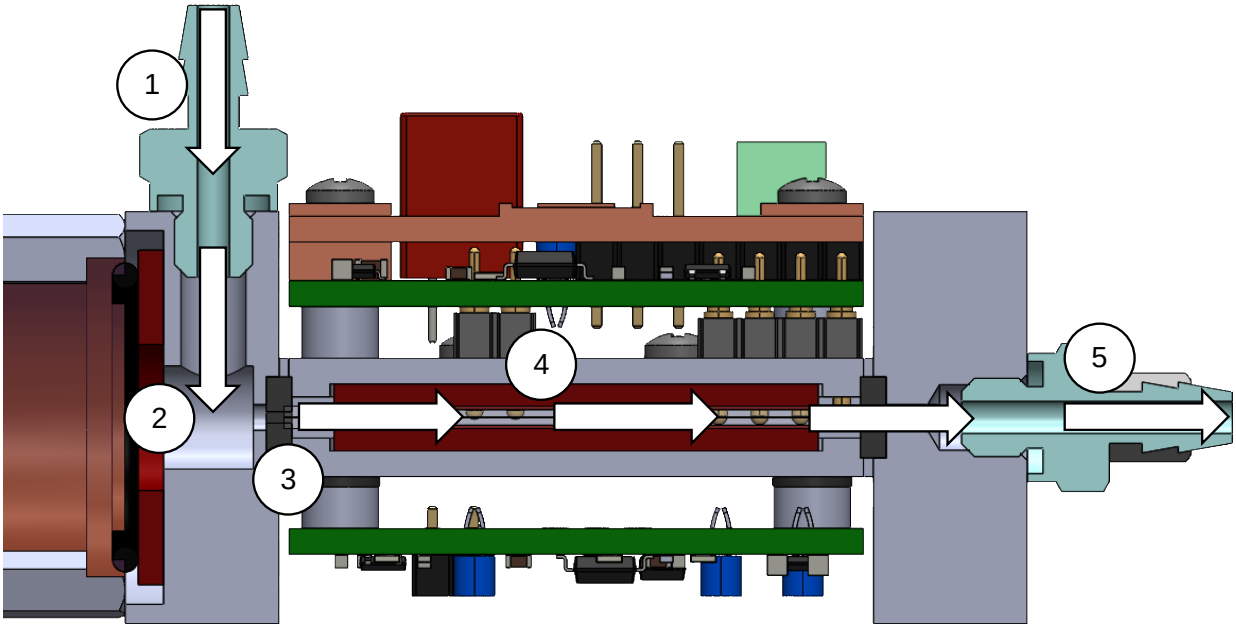

Figure 5. Assembled detector cross section

(1) Side cross section view of the assembled Detector detailing the flow path; (2) Sample gas is introduced at the inlet; (3) The sample is then ionized by the UV bulb; (4) Ionized sample flows into the device; (5) Ion species are attracted to their respective detector electrode and ion neutralization induces a current that is converted into a voltage signal by the circuitry; (6) Sample exits the device through the outlet.

2.3 Electronics Architecture

The detector system electronics are comprised of two symmetric printed circuit boards mounted on each side of the fixture. This two-PCB system facilitates a highly configurable ion detection scheme allowing for positive and negative mode ion sensing either independently or simultaneously. For the most versatility, there are physical jumper pins that allow the bias voltage of the PCB to be set to be negative, positive, ground, or digital mode. The digital mode setting enables microcontroller control of the voltage bias and thus enabling remote control of the detector operation mode. The schematic illustrates this in **Figure 6**. The digital mode is facilitated by using a switch package (Texas Instruments, Dallas, TX) that is compatible with both 3.3 and 5 V digital control inputs covering the great majority of readily available microcontroller platforms.

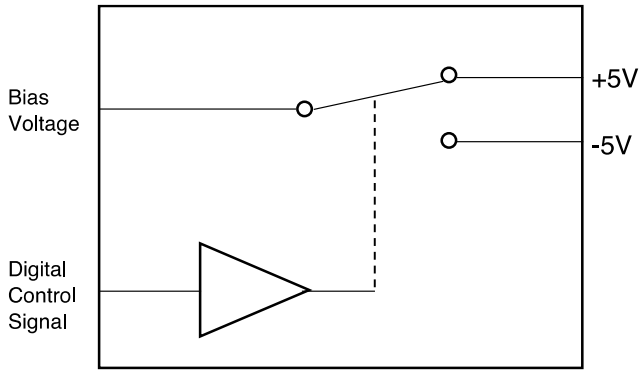

Figure 6. Bias voltage digital selection circuit

2.3.1 Battery Power

For the electronics to function off battery power, a power architecture was designed to supply the sensitive components with very low noise voltage. The architecture of the power network fully powered off one 9 V battery is shown in **Figure 7**. The step-up/down regulator S18V20F9 (Pololu,

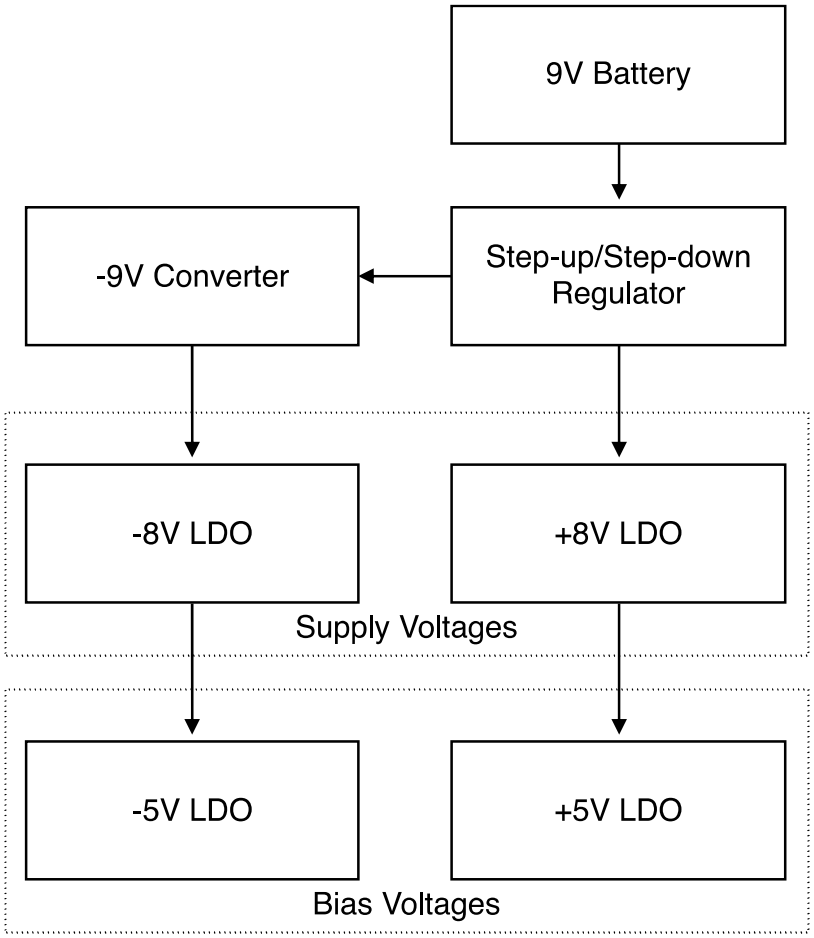

Figure 7. Battery Power System Architecture

Las Vegas, NV) ensures a stable voltage as battery voltage can vary from battery to battery and throughout the life of a single battery as the voltage tends to decrease as it nears empty (**Table 1**). A DC/DC converter allows for negative voltages that are subsequently regulated with low-noise LDO (low-dropout) regulators that provide extremely stable voltage supplies for the integrated circuit (IC) device on the PCB and for the bias voltages as well. The resulting current draw of the system is approximately 25 mA. Given that the capacity of 9 V batteries is typically

around 500 mAh, the system can easily last an entire day of non-stop field work and could potentially last over several days with intermittent operation.

Table 1. Detector Stability

Current draw, baseline average taken over a 10 second interval, and standard deviation presented for a range of supply voltages to simulate battery voltage level fluctuations.

Supply (V)	Current (mA)	Baseline (V)	σ
7.50	26.8	6.185	0.0048
7.75	26.4	6.190	0.0048
8.00	26.0	6.193	0.0056
8.25	25.6	6.185	0.0042
8.50	25.3	6.184	0.0043
8.75	24.9	6.191	0.0053
9.00	24.5	6.187	0.0042
9.25	24.2	6.186	0.0057
9.50	23.8	6.184	0.0043

2.3.2 Signal Conditioning

Currents from trace chemical concentrations are often in the picoamp and as low as the femtoampere range. The careful design of the amplification circuits and layout of the physical boards is imperative to mitigate signal leakage. The amplification electronics for the detector module are arranged in two stages as depicted in **Figure 8**. The first stage is comprised of a transimpedance amplifier with an extremely high gain set by the gain resistor RH73X2A50GNTN (TE Connectivity, Schaffhausen, Switzerland). The second stage uses an instrumentation amplifier to further amplify the converted voltage signal and to remove the bias voltage from the output. This stage provides signal conditioning configurability such that the output can be

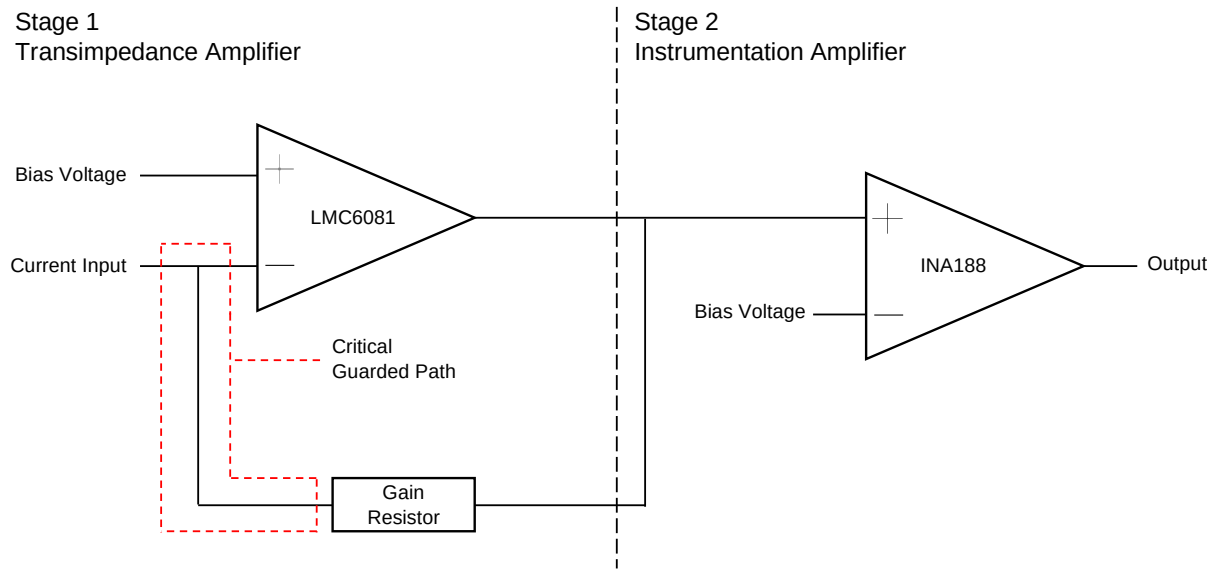

Figure 8. Signal amplification and conditioning circuit

measured by either a handheld digital multimeter or for integration into a microcontroller-based system. The gain of the instrumentation amplifier INA188 (Texas Instruments, Dallas, Texas) is set by a single external resistor and can be set from 1 to 1000. In the reported experiments, the gain of the second stage was set to 6.

Low-level sensing electronics are highly sensitive to electromagnetic interference (EMI). Since multiple layers of shielding is more effective than a single shielding layer [52], two components of grounded metal shielding are implemented to minimize electrical noise. The inner shielding layer is comprised of the copper shielding plate. During experiments, the entire detector is placed in a grounded metal housing further protecting it from EMI.

It is critical to minimize leakage current paths when considering the board layout of the transimpedance amplification stage for picoamp-level sensing. Surface charge and surface contaminants can potentially contribute to tens of picoamps of current leakage severely degrading the detection limit of the electronics [53]. In this detector, several techniques are implemented to minimize current leakage of the input to the amplifier. One technique is surrounding the input path

with a guard that is held to the same voltage as the amplifier input such that the surrounding conductors do not facilitate leakage. This is implemented both on the device level and on the circuit board electronics level. On the device level, the guard is a powered trace that surrounds the detector electrode. On the circuit board level, the input current path (**Figure 9**) to the transimpedance amplifier is enclosed by a continuation of that powered guard trace. The guard is actively driven to the same voltage level as the amplifier input and is sourced as the bias voltage. Another technique is for surface charge mitigation, the input trace area is void of solder mask to eliminate leakage current path through the solder mask. Finally, to mitigate leakage paths from surface contamination, PCBs were cleaned in an ultrasonic bath with saponifying cleaner to remove common contaminants such as residual flux and fine particulate. The cleaning procedure is detailed in Appendix A: Cleaning of Assembled Detector PCB Procedure.

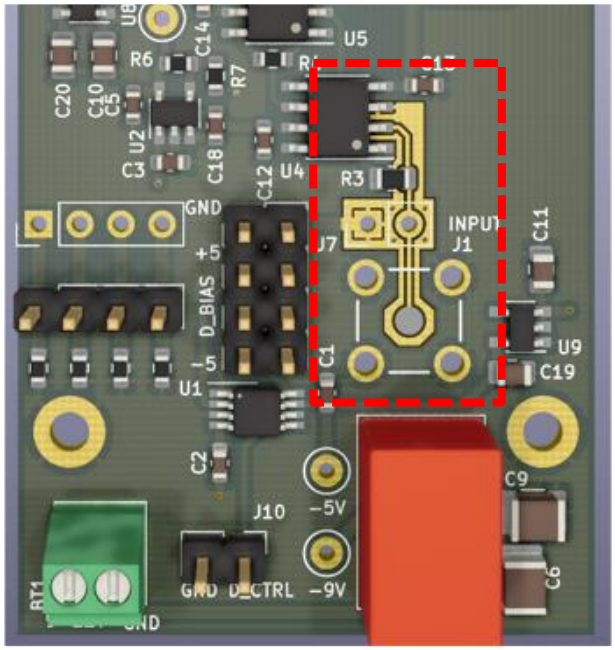

Figure 9. Detector input current path

Rendering of the detector electronics PCB highlighting the guarded signal input path.

2.4 Results and Discussion

The setup to measure trace chemicals with the detector is shown (**Figure 10**, A). House compressed air is filtered (Restek, Bellafonte, PA) and serves as the carrier gas. The air is metered at 200 mL/min using a mass flow controller (Alicat Scientific, Tuscon, AZ). The carrier flow is combined with the sample at a tee (Swagelok, Solon, OH). Chemical samples were prepared [54] at 1000 ppm for each chemical species in a Tedlar gas sampling bag (Sigma-Aldrich, St. Louis, MO). A gas tight 10 mL syringe (Hamilton Company, Reno, NV) is filled with the sample and the flow is metered with a syringe pump (Harvard Apparatus, Holliston, MA) to augment the resulting trace concentration of the chemical that comes out of the tee. Keeping the carrier gas flow constant, chemical sample with varied concentrations were injected into the detector system. Directly at the outlet of the tee, the mixed sample and carrier gas is transported

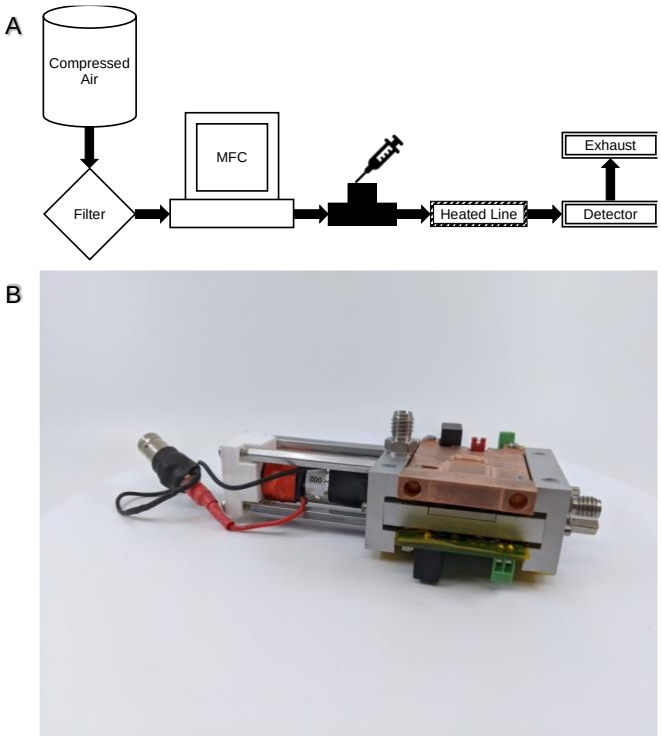

Figure 10. Assembled detector
(A) Schematic depiction, and (B) photograph of the assembled detector.

with a heated stainless steel metal tubing line. A temperature controller (Omega Engineering Inc., Norwalk, CT) with PID control was used to achieve the gas heating with a setpoint of 90 ºC. Temperature fluctuations will affect ion mobility based chemical results and signal intensity. To avoid this, we kept the temperature at a stable level by allowing the detector assembly with the carrier gas to stabilize at an experimented temperature with the control of the temperature of the heated inlet line. Signals were reproducible with such conditions. Usually, temperature fluctuations of ±2 degree or less contribute negligible impact to an ion mobility chemical signal and its intensity [55]. Our data was obtained within those limits. Prior to testing with chemical samples, the entire module was leak tested with helium gas at 10 mL/min to confirm flow through the sensing device and to prevent any hazardous chemicals from leaking into the environment.

2.4.1 System Step Response

To measure the step input response of the system, 1 ppm acetone was injected at a constant rate. Then at manually controlled intervals, the ionization source (UV) was switched on resulting

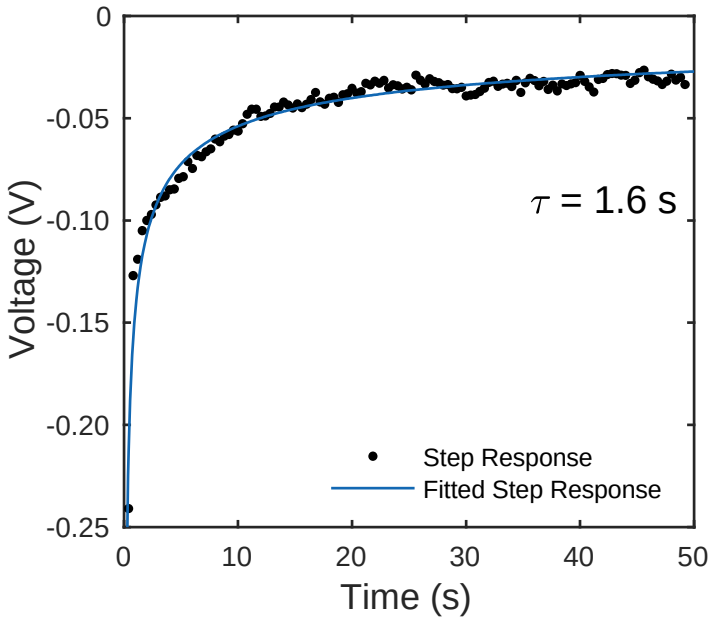

Figure 11. Detector output response to step input

in the rise shown in **Figure 11** and kept on until a steady state is reached and then switched off. This was repeated for four replicates. One of the replicates is plotted and shown in **Figure 11**. The response time was then calculated as time elapsed to reach a signal value -3dB from the stabilized maximum value. The step response time constant τ was found to be 1.6 seconds. This is nearly half the value of the battery-operated electrometer reported in [37] where the step response was measured in an ideal configuration.

2.4.2 Detection of Trace Chemicals in Dual Polarities

The linearity and detection capability of the system was examined for several chemicals. The syringe pump volume flow was varied to produce different concentrations ranging from 100 to 10000 ppb while keeping the carrier gas flow constant at 200 mL/min. Injections were performed for several positive mode (toluene, xylene and acetone) and negative mode (acetone and methyl salicylate) chemicals. The injections for each concentration were performed in triplicate (n=3). Due to background noise and other environmental factors, there is an offset in the signal that

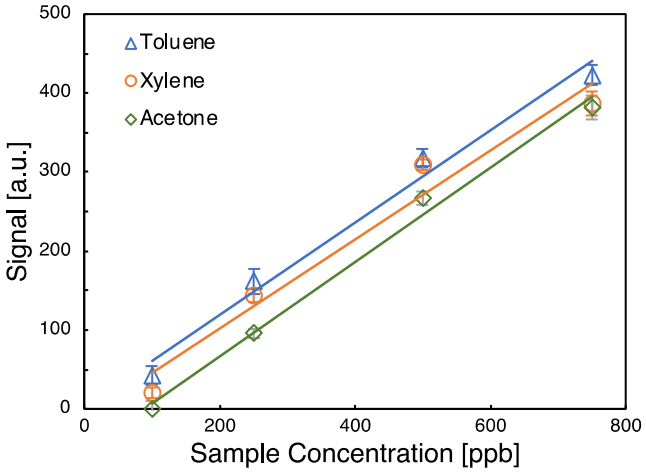

Figure 12. Positive mode signal response

Signal response in a.u. (arbitrary units) for positive mode chemicals versus the concentration (100, 250, 500, and 750 ppb). The R^2 values are 0.98, 0.97, and 0.99 for toluene, xylene, and acetone respectively. Vertical error bars represent the standard deviation of three replicates.

results in a non-zero baseline value. This can be automatically corrected by taking a baseline measurement that is then used to subtract from subsequent measurements. The positive mode chemicals (**Figure 12**) were each measured at the same corresponding concentrations from 100 to 750 ppb and the results show highly linear responses. The negative mode responses for acetone and methyl salicylate were also highly linear. Methyl salicylate was found to have a much lower signal to concentration ratio compared to acetone. The results of the negative mode

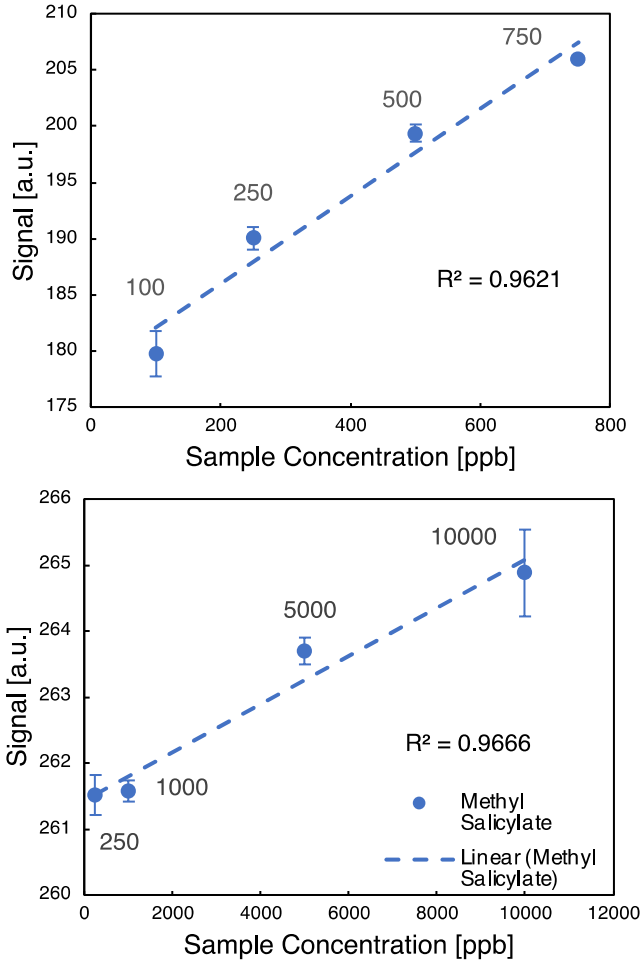

Figure 13. Negative mode signal response

Signal response for negative mode detection of two chemicals. Top panel shows linearity for acetone. Bottom panel shows signal at a much wider range of concentration still has a linear trend. The signal response slope with increasing concentration for methyl salicylate in negative mode detection was significantly lower than acetone.

responses are plotted separately (**Figure 13**). The response of acetone was measured at concentrations from 100 to 1000 ppb and showed highly linear responses like that of the positive mode measurements. Methyl salicylate was measured at concentrations from 250 to 10000 ppb. The results are still highly linear but less than that of measurements taken from a smaller range of concentrations which is to be expected. This illustrates the potential for this system to be used for detection of a wide range of concentrations.

2.5 Conclusion

A low powered dual-polarity portable ion detector was developed and demonstrated to detect trace level chemicals. The detector electronics allow for both manual and digital control of the ion sensing polarity mode. Ion species of both positive and negative polarity were sensed at trace levels down to 100 ppb. The output of the detector in both modes showed linear responses proportional to the chemical concentrations tested. Chapter 3 will explore the great promise in integrating this detector in series with other analytical techniques such as gas chromatography (GC) and ion mobility spectrometry (IMS) to add dimensionality to the analysis. The low current draw and small form factor makes the system amenable for integration into field portable systems. Furthermore, with the integration of a desorption unit and the use of a higher energy ionization source, the detection of negative ion yielding compounds, such as explosives, may be explored.

Chapter 3: Portable chemical detection platform for on-site monitoring of odorant levels in natural gas

The adequate odorization of natural gas is critical to identify gas leaks and to reduce accidents. To ensure odorization, natural gas utility companies collect samples to be processed at core facilities or a trained human technician smells a diluted natural gas sample. In this chapter, we report a platform utilizing the detector work from Chapter 2 to addresses the lack of mobile chemical detection platforms capable of providing quantitative analysis of mercaptans, a class of compounds used to odorize natural gas. Detailed description of the platform hardware and software components is provided.

Designed to be portable, the platform hardware facilitates extraction of mercaptans from natural gas, separation of individual mercaptan species, and quantification of odorant concentration, with results reported at point-of-sampling. The software was developed to accommodate skilled users as well as minimally trained operators. Detection and quantification of six commonly used mercaptan compounds (ethyl mercaptan, dimethyl sulfide, n-propylmercaptan, isopropyl mercaptan, tert-butyl mercaptan, and tetrahydrothiophene) at typical odorizing concentrations of 0.1 – 5 ppm was performed using the device. We demonstrate the potential of this technology to ensure natural gas odorizing concentrations throughout the distribution pipelines.

The detection platform integrates custom software and hardware as depicted in **Figure 14**. The custom software is comprised of embedded microcontroller code and a Python-based graphical user interface (GUI) program. The microcontroller code takes inputs from the GUI program to actuate the hardware then takes sensor readings to update the GUI data and display. The GUI program provides a user interface to set run parameters. The GUI also provides a way to save

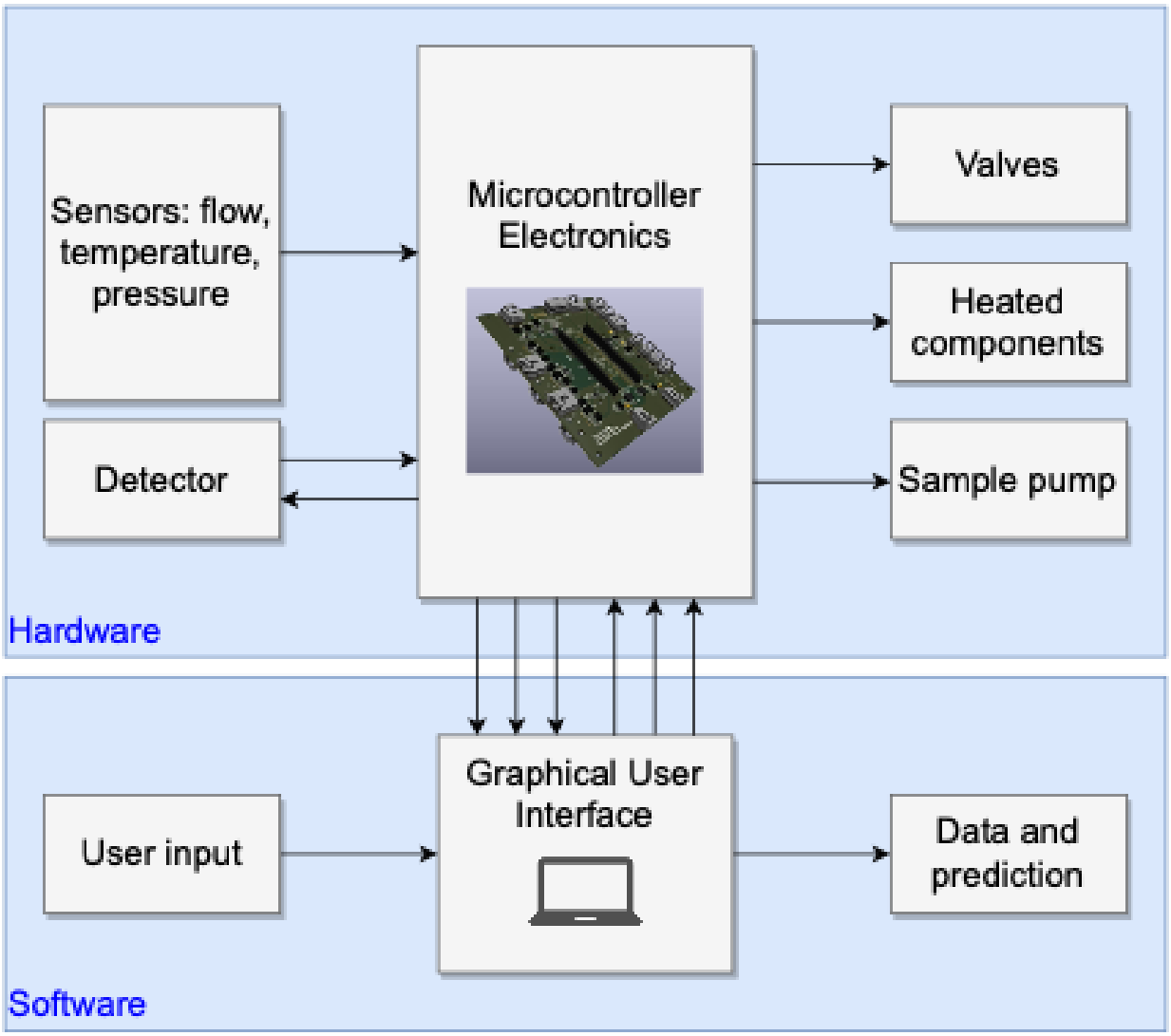

Figure 14. Overall platform architecture

The arrows show the general flow of data and control. As inputs, the microcontroller takes sensor and detector data. As outputs, the microcontroller communicates with the detector and controls platform hardware including valves, heated components, and the sample pump. The Graphical User Interface program takes user input for method parameters while saving data and providing compound prediction capabilities.

data and to provide a prediction of sample mercaptan concentration. The hardware components facilitate the main functions of the platform, all within a single assembly: the extraction and preconcentration of mercaptans from a natural gas sample, the chromatographic separation of individual mercaptan species, and the detection of odorant compounds.

3.1 Custom Software

There are two principal components that make up the platform software: the embedded microcontroller code and the GUI. The embedded microcontroller code runs on an Arduino based development board (Teensy 3.6). The embedded code facilitates all the hardware functions of the flow control system. Digitized readings from the sensors and the detector are saved as an interaction between the embedded code and the GUI. **Table 2** and **Table 3** summarize the microcontroller communication protocol inputs and outputs respectively.

Table 2. Table of Microcontroller Inputs

Component	QTY	Type	Protocol	Reference Circuit
Main Flow Sensor	1	analog	analog	S 4-2
GC Flow Sensor	1	digital	I2C	S 4-2
Sample Flow Sensor	1	analog	analog	S 4-2
Pressure Sensor	1	analog	analog	S 4-2
GC column RTD	1	digital	SPI	S 4-3
Heated Line Thermocouple	3	digital	SPI	S 4-3
Trap Thermocouple	1	digital	SPI	S 4-3
Detector Waveform Amplitude	2	analog	analog	S 4-4
Detector Signal	1	digital	SPI	S 4-4

Table 3. Table of Microcontroller Outputs

Component	QTY	Type	Protocol	Reference Circuit
3-Way Valve	2	digital	I/O	S 4-2
3-Way Valve	1	digital	I/O	S 4-2
Proportional Valve	2	digital	SPI	S 4-2
Sample Pump	1	digital	I/O	S 4-2
GC Column Heater	1	PWM	-	S 4-3
Heated Line Heater	3	PWM	-	S 4-3
Trap Heater	1	PWM	-	S 4-3
Detector Module Enable	5	digital	I/O	S 4-4
Detector Module Waveform	1	digital	I2C	S 4-4

The GUI is a Python-based program that provides the operator with capabilities to control the hardware and to perform analysis on natural gas samples. The parameters of each method run are set through the GUI. These parameters are sent to the microcontroller, executing the sequence of events automatically. Subsequently, detector data is streamed to the GUI. Finally, an odorant concentration estimation is produced with the run data. This prediction is based on the data analysis method described later in this chapter. GUI tabs are depicted in the appendix,

Appendix B: Graphical User Interface (GUI) Tabs.

3.2 Platform Hardware

The platform hardware is largely comprised of commercial-off-the-shelf (COTS) components which are detailed in Appendix C: List of Materials. The chassis for the platform is constructed from laser cut acrylic panels and held together with standard fasteners. The platform hardware has been arranged into three layers as depicted in the exploded 3D model (**Figure 15**). The hardware components are affixed on an acrylic panel that are housed in the chassis. The custom

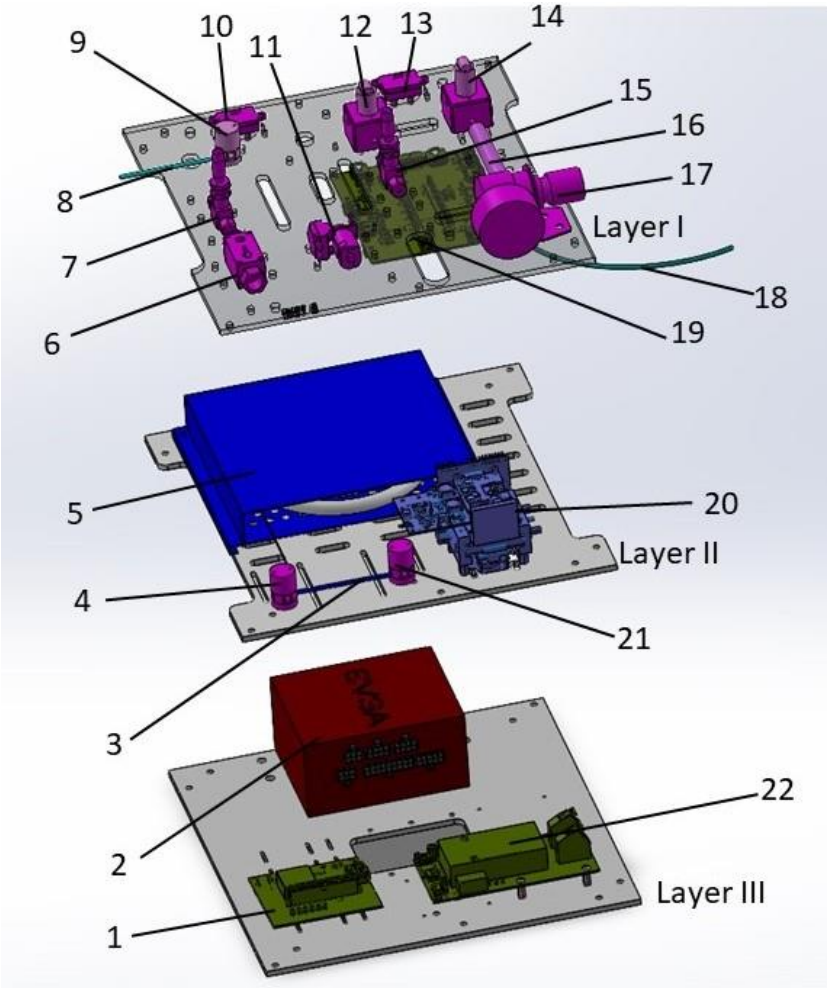

Figure 15. Platform 3D Model

The platform is comprised of 3 stacked layers – Layer I: flow control, Layer II: analysis, Layer III: power. The parts are numbered as follows: 1 main power electronics; 2 device power supply; 3 silica gel trap; 4, 9, 21 2-way valves; 5 GC; 6 natural gas sample flow sensor; 7, 15 needle valve; 8 sample inlet; 10, 13 flow sensors; 11 sample pump; 12, 14 proportional valve; 16 filter; 17 nitrogen pressure regulator; 18 nitrogen inlet; 19 device control electronics; 20 detector; 22 ionization power electronics. Components are color coded – purple: flow, green: electronics, blue: analysis.

electronics are implemented with printed circuit boards (PCB) that were designed in KiCad. The circuit schematics are detailed in Appendix D: Electronics Circuit Schematics. The platform chassis dimensions are roughly 300 $\times$ 290 $\times$ 290 mm. The full hardware assembly weighs approximately 6 kg. In the following sub-sections, key hardware components are described in detail organized by layer.

Layer I: Flow Control

The components responsible for sampling and control of the desorption and supplemental nitrogen flow are positioned on Layer I of the hardware assembly. These components direct the flow of sample through the analysis components and control the flow of supplemental carrier gas throughout the platform hardware. The platform is designed to handle the introduction of natural gas samples in two scenarios: (1) sample can be drawn directly from a natural gas line provided it has been regulated down to less than 1 psi or (2) sample can be drawn from a passive carrier vessel (e.g., Tedlar bag or inert canister). The sample pump (KNF, NPM015) (**Figure 15**: 11) is connected to either the sample inlet or atmosphere through a 3-way valve (Clippard, NR1-3M-12) (**Figure 15**: 9). The sample flow rate is manually controlled downstream through a needle valve (Swagelock, SS-SS2) (**Figure 15**: 7) and is measured by a natural gas flow sensor (OMRON, D6F-01N2-000) (**Figure 15**: 6). The supply of ultra-high purity (UHP) nitrogen gas (AirGas, UHP300) (**Figure 15**: 18) is introduced through a pressure regulator (McMaster, 6763K81) (**Figure 15**: 17). The regulator protects the downstream components that have specified pressure limits. Moreover, the UHP nitrogen goes through an additional filter (Valco, ZUFR2) (**Figure 15**: 16) to prevent particles larger than 2 mm from reaching sensitive components. The overall flow rate of nitrogen is controlled by a proportional valve (Norgren, D170.0004) (**Figure 15**: 14). A flow sensor (Honeywell, HAFBLF0750C4AX5) (**Figure 15**: 13) provides feedback for overall flow control. At the proportional valve (Norgren, D170.0004) (**Figure 15**: 12), the flow splits into two branches: the desorption flow and the make-up flow. The desorption flow carries the sample through the analysis components. The make-up flow supplements the desorption flow into the detector. This supplemental flow is modulated by another needle valve (**Figure 15**: 15), enabling the proportional valve control of desorption flow to operate within a specified range.

Layer II: Analysis

Layer II contains the elements of the platform related to heating and sample analysis. The sorbent-packed trap (**Figure 15**: 3) between the 3-way valves (Clippard, NR1-3M-12) (**Figure 15**: 4 & 21) is used to extract the odorant compounds from natural gas samples allowing for larger sampling volumes while retaining odorant compounds on the silica gel sorbent. Prior to development of the sensor platform, a study was conducted to determine the appropriate sorbent material for the extraction and preconcentration of odorant compounds from natural gas. It was found that usage of a preconcentrating trap greatly increased detection sensitivity of the sulfur odorant compounds used in natural gas production and silica gel was the most sensitive as measured by signal per milligram sorbent. Additional details of this study can be found in supplemental material of the published article [56]. Thus, a preconcentrating trap packed with silica gel sorbent was used. The sorbent traps are constructed with a stainless-steel tube that has been treated with Sulfinert® (SilcoTek, Bellefonte, PA) which passivates the tubing surface with a layer of amorphous silicon. This treatment addresses a challenge of measuring reactive sulfur compounds, which tend to adsorb to untreated surfaces [57]. The construction for the trap component is a modified version of the heated transfer line assemblies as described in Appendix E: Heated Line Construction Procedure. Before the fittings are placed, silica gel sorbent is packed into the trap and held in place by steel mesh frits.

Gas chromatography (GC) is used to separate the individual odorant compounds. The transit of the sample and the resultant retention peaks strongly depend on the temperature profile from sampling to detection. Due to this, the entire analysis flow path is typically housed in a high-power GC oven. This presents a challenge for mobilizing GC capabilities in a portable platform.

This challenge is addressed by utilizing controlled directed heating to the critical flow paths. For the GC column, a “low thermal mass” (LTM) GC column, type DB-624, 30 m × 0.32 mm × 1.80

µm (Agilent, 123-1334LTM) (**Figure 15**: 5) is employed. These commercially available GC modules provide “ultrafast temperature programming with an unprecedented cool down time and low power consumption” [58] that is characteristic of Low Thermal Mass Gas Chromatography (LTMGC). For the sample flow paths entering and exiting the GC column, heated transfer line assemblies were constructed in-house to directly heat the critical flows. There are a total of three heated transfer line assemblies that are set to hold at a constant temperature of 100 °C. The construction method for the heated transfer line assemblies is detailed step-by-step in Appendix E: Heated Line Construction Procedure. The first connects the sorbent trap to the GC, heating the GC inlet flow. The remaining two heated transfer lines are assembled on a make-up adapter (Valco, MUA) where one heats the nitrogen at the supplemental make-up flow inlet and the other heats the body of the make-up adapter that connects the outlet of the GC column to the inlet of the detector (**Figure 15**: 20). Additionally, the detector component is also heated to a constant temperature with a heater constructed of resistive wire embedded into silicone.

The detector component (**Figure 15**: 20) is a progression of the detector system described in Chapter 2. This version features separation waveforms generated by a boost converter and RF amplifier controlled in tandem by several digital potentiometers. The circuit schematics and explanation of the waveform generation electronics are detailed in supplemental material of the published article [56]. This operates according to the principal of ion mobility, whereby mercaptan ions are manipulated in a drift tube with oscillating, asymmetric energy fields, and then subsequently interact with the detector electrode to generate an electrical signal [59], [60]. This

detector component runs off a single 12 V supply allowing for it to be operated as a standalone device or as in this work, a platform integrated detection module.

The detection module electronics and the microfabricated sensor device are an adaptation of the work detailed in Chapter 2 and is also described fully in published work [61]. The main physical modification is the location of the ultra-violet (UV) ionization source which was relocated to bottom of the fixture. This required an opening to be drilled in the bottom glass plate of the detector flow path to allow UV light to pass through for ionization. The revised device layout is illustrated in **Figure 16** and depicts the opening (UV BULB INLET) that was drilled on one of the device's chip halves.

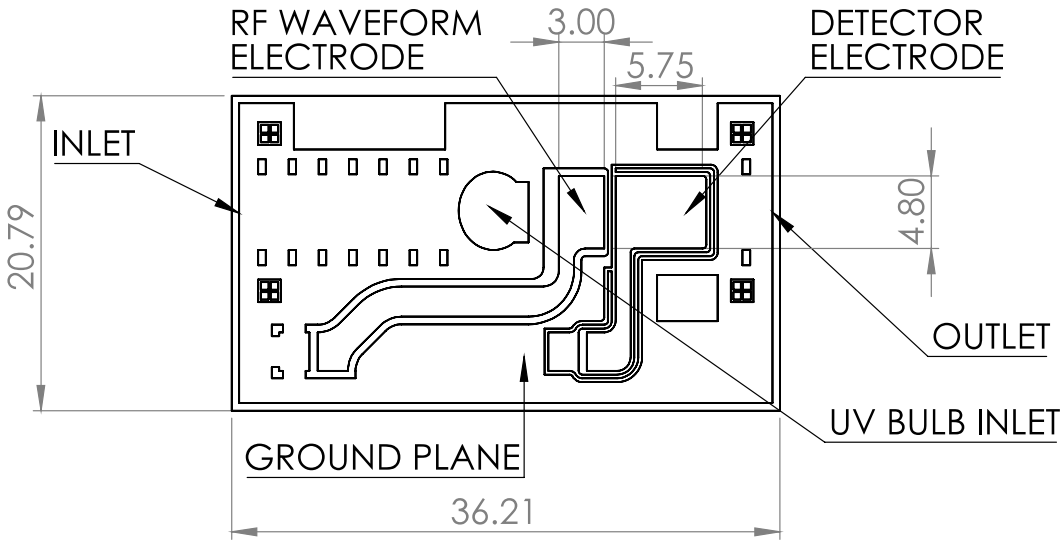

Figure 16. Drawing of Gas Sensor Device

Layer III: Power

The power distribution architecture was designed to enable mobile deployment of the platform. A compact computer power supply (EVGA SuperNOVA 450 GM) serves as the main power supply and is integrated into the chassis on the bottom layer of the platform assembly. This power supply provides a robust source for commonly required voltage levels for the platform electronics while allowing the platform hardware to be powered by a single standard AC power cord. The main power electronics (**Figure 15**: 1) facilitate power distribution to the platform hardware components, and the circuit schematic is detailed in Appendix D: Electronics Circuit Schematics. Powering the UV bulb ionization source posed a unique challenge as high voltage levels (>1 kV) are required to ignite the Krypton lamp [62]. The High Voltage Power Supply (HVPS) module was designed to address those requirements. The HVPS is an isolated electronics module that powers the bulb safely while mitigating potential electromagnetic interference (EMI). In addition to a manual switch, the HVPS can be controlled digitally such that the main controller electronics can power the ionization source on and off removing the need for physical contact with the high voltage electronics. The circuit schematic for the HVPS is provided in Appendix D: Electronics Circuit Schematics.

3.3 Platform Operation

The platform operation can be generalized into two modes as depicted in **Figure 17**. Each mode is summarized in this section while the specific parameter values will be detailed in the following section.

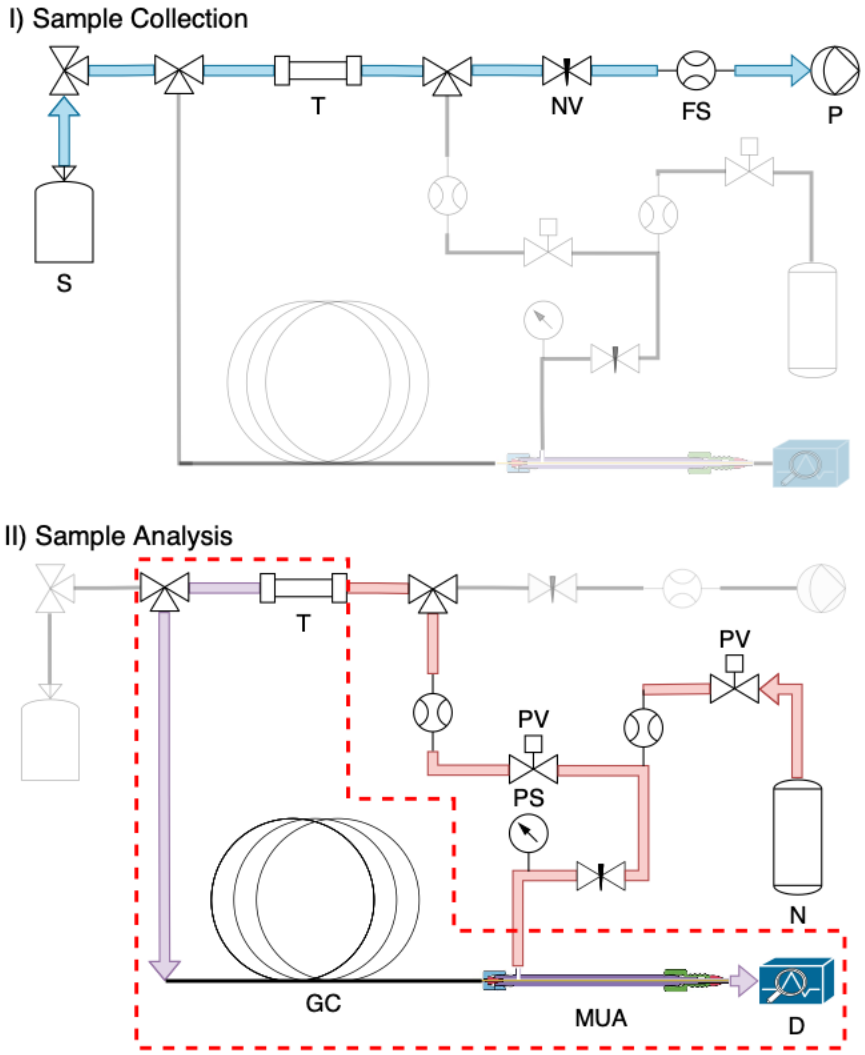

Figure 17. Hardware schematic.
I) Sample flow path is light blue. II) Nitrogen flow is light red. Sample flow carried by nitrogen is violet. Active heating is indicated by the dashed line. Legend: **S** sample inlet; **T** silica gel trap; **NV** needle valve; **FS** flow sensor; **P** sample pump; **PV** proportional valve; **PS** pressure sensor; **N** nitrogen; **GC** gas chromatography column; **MUA** make-up adapter; **D** detector.

3.3.1 Sample Collection

During the sample collection mode, the natural gas sample source is attached to the sample inlet. Then the sample pump pulls the sample through the sorbent trap, concentrating the mercaptans onto the sorbent. The needle valve downstream of the trap provides a tunable parameter for the flow rate of sampling collection. The sampling time set through the platform GUI software, provides an additional tunable parameter for this mode of operation.

3.3.2 Sample Analysis

During the sample analysis mode, three-way valves are actuated such that nitrogen gas from a pressurized cylinder drives the gas flow. The sorbent trap is heated to the desorption temperature to release the preconcentrated sulfur compounds. Simultaneously, the desorption flow is increased during the trap heating, so there is minimal separation of compounds before the sample reaches the GC column inlet. Then, the desorption flow is held steady at a lower rate for the rest of the analysis period. Following the GC column, a fused silica make-up adapter (VICI, Houston, TX) connects the column outlet to the detector. The make-up adapter facilitates the addition of an auxiliary nitrogen flow for the separated mercaptans as they elute from the GC column and into the detector. The rates of the GC flow and make-up flow are set by a combination of two proportional valves and a manual needle valve. The two proportional valves are electronically controlled allowing for a control scheme to be implemented in the embedded software. After the analysis mode is complete, the raw data is processed by the GUI, which provides the quantitative concentration values for individual mercaptan species.

3.4 Analytical method

Natural gas distribution lines are odorized with approximately 1 ppm concentration mercaptans [16], which was used as the target concentration for optimization. Prior to development of this portable platform, optimization experiments for certain analytical parameters were performed on a commercial platform to achieve target mercaptan sensitivities with minimal sampling times. Select optimization parameters are detailed in the supplemental material of the published article [56].

The following method was used on the portable platform. At the initiation of sample collection (t=0 s), the silica gel trap was held at 35 °C, sampling for 60 seconds at a rate of 60 mL/min. The trap was then flushed with ambient air for 5 seconds to purge residual natural gas from the trap. Sample analysis began at t=67 s and when the trap was heated to 180 °C for 170 seconds. Next, 5 mL/min flow of ultra-high purity nitrogen carried desorbed mercaptans through the GC column, which was maintained at 40 °C. At t=127 s, the flow through the GC column was reduced to 1 mL/min. At t=1045 s, the GC column was then heated to 160 °C at a rate of 25 °C/min, holding until 1650 s to speed up the release of the final expected compound, THT.

The GC column eluent was mixed with a 600 mL/min auxiliary flow of nitrogen into the ionization and detector module. The detector fixture was set to 35 °C and scanned from -2 to 2 compensation voltage (CV) with the separation voltage (SV) set to 0 V to maximize sensitivity.

3.4.1 Standards and Sample Preparation

Odorant samples were prepared by diluting pure mercaptan standards in 10 L Tedlar bags with nitrogen balance at precise concentrations. Commercial standards of ethyl mercaptan (ETM), dimethyl sulfide (DMS), n-propylmercaptan (NPM), isopropyl mercaptan (IPM), tert-butyl mercaptan (TBM), and tetrahydrothiophene (THT) were purchased from Sigma-Aldrich

(Burlington, MA). Ultra-high purity nitrogen gas was obtained from AirGas (Radnor Township, PA). Tedlar bags were from Restek Corporation (Bellefonte, PA).

The ideal gas law was used to calculate the required liquid volume from the original vials for preparation of the stock mixture concentration of 1000 ppm v/v in nitrogen balance. Serial dilutions were made using additional Tedlar bags to achieve target concentrations.

3.4.2 Sensor calibration and data analytics

Data generated by the detector is three dimensional, with the x-axis representing compensation voltage (CV, measured in volts), the y-axis representing retention time (RT, measured in seconds), and the z-axis representing signal intensity (measured in volts). Raw data underwent standard chemometric preprocessing techniques, specifically baseline removal, as available in our previously reported AnalyzeIMS software [54], [63]–[66], a custom software package to process and interpret differential mobility spectrometry data streams.

To quantify odorant concentration readings, the peak volume for each odorant compound (with a specific RT) was calculated by summing the signal corresponding to RT $\pm$ 10 s and CV values from –0.5 V to 0.5 V. The sensor platform was trained on n=3 samples of each mercaptan at five concentrations (0.1, 0.5, 1, 3, and 5 ppm). Linear regression was applied to the experimental data to obtain the calibration curve/model used to predict the compound concentration of natural gas samples. Once the required model parameters (slope and y-axis intercept) were obtained for each of the odorant compounds, the peak volumes of samples with unknown concentrations were fed into the model to predict the concentrations of individual odorant compounds.

3.5 Results and Discussion

3.5.1 Portable Analysis Platform Performance

Power Consumption

To gauge the power consumption of the platform hardware in practice, we attached a power meter (Kill A Watt® EZ, P3 International) to the platform power supply. Each run from sampling to completion averaged 30 Wh (this measurement was limited by the resolution of the power meter). This is significantly lower than the power required to run such an analysis on a traditional laboratory GC. With the low power requirements, it would be possible to run the platform hardware off a mobile generator or battery pack. For example, 500 Wh mobile battery packs are readily available for purchase and would be able to power the platform hardware to perform roughly 17 analysis runs.

Heat and Flow Control

Each of the heated transfer line assemblies followed a proportional control scheme for the pulse width modulated (PWM) control of the heater current but are capable of PID control with adjustments to the embedded code. The proportional gain results in supplying the full supply voltage to the heaters when temperature is below 4.1 °C of the target value and decreases PWM duty cycle linearly with the temperature error, which allowed the heated assemblies to heat up quickly and maintain stable temperature control at the target value. This is especially important for the trap which ideally would heat up as a step function to release the preconcentrated compounds rapidly from the sorbent. Our implementation resulted in the trap reaching 90% of the target 150 °C within a mean time of 14 s (standard deviation, or SD=0.69). The heated assemblies also had very consistent temperature profiles throughout 25 runs during which calibration curve data was obtained. Supplemental plots of the 25 temperature profiles

superimposed on a single set of axes visually confirms the repeatability of the temperature controls (Appendix F: Temperature and Flow Data).

Controlling the flow rate proved challenging. PID closed-loop control was implemented for the proportional valves to augment the flow to track commanded flow rates for the desorption flow and the carrier make up flow. There were several factors that contributed to the challenge of flow control for the platform. The proportional valves used as the main actuator for the flow control had a non-linear response in a great portion of the minimum and maximum controllable range, as well as significant hysteresis during control direction changes. The needle valve was manually tuned to ensure the flow rates were achievable within the controllable operating range of the proportional valve. The resolution accuracy of the flow sensors was also an issue as we found there were inconsistencies with the readout of the flow sensors. Plots (Appendix F: Temperature and Flow Data) of the flow and pressure data show that the make-up flow was well controlled. There is significant high frequency variation seen in the plots of the desorption flow due to the combined factors of the flow sensor resolution at low flows and the limited control capabilities of the proportional valves. However, the average desorption flow over the course of an individual analysis followed the commanded values of 5 mL/min for desorption and 1 mL/min for GC column elution acceptably. The mean flow values for n=25: desorption 4.95 mL/min SD=0.48 and elution 1.01 mL/min SD=0.05.

For future work to improve the platform, there are several avenues to explore. One would be to decouple the desorption flow from the make-up flow. In this work, both controlled flows are derived

from a single source flow. The source flow could be split but carries a tradeoff of requiring more components to isolate the two flows.

Despite these challenges, the flow control system performed consistently run-to-run, with average flow values matching the commanded values. More importantly, the application performance discussed in the following sub-section shows the potential for this platform.

3.5.2 Application to Natural Gas Odorant Compounds

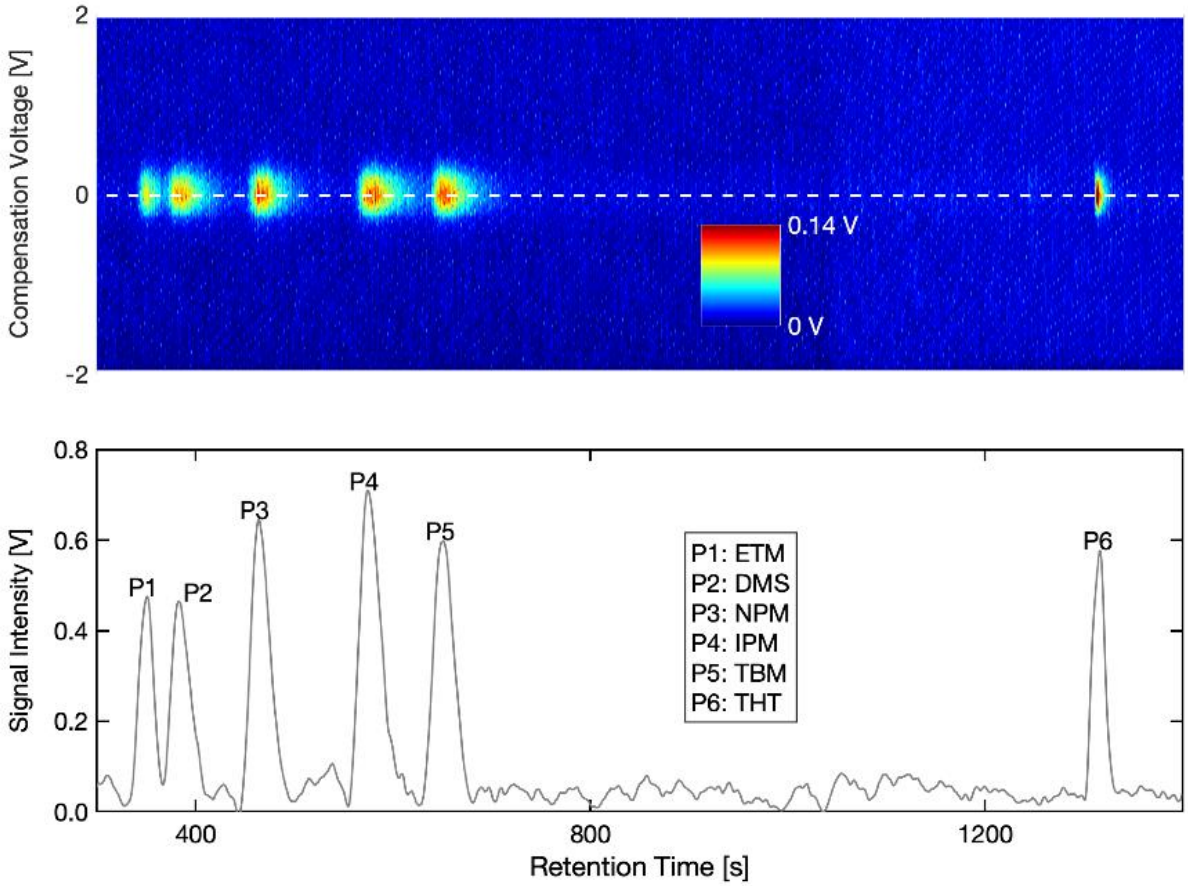

Figure 18. Sample detection signal

Detection signal from a sample containing the six mercaptan analytes. (top) Raw signal, showing the three dimensionality of the detector data. (bottom) Side view of the detector data.

The detection and quantification capabilities of the platform were examined for a mixture of 6 mercaptan compounds found in three odorant blends commonly used in the natural gas industry (Spotleak 1009, 1039 and 1420). The six mercaptans included ethyl mercaptan (ETM), dimethyl sulfide (DMS), n-propyl mercaptan (NPM), iso-propyl mercaptan (IPM), tert-butyl mercaptan (TBM) and tetrahydrothiophene (THT). An example chromatograph is provided in **Figure 18** and shows the detection signal from a synthetic sample containing all six mercaptans. Mercaptans were separated by the GC column, affording individual measurements and quantification of each compound. Peaks exhibited a symmetrical shape, with widths at half prominence ranging from 12.97 seconds (THT) to 36.25 seconds (TBM).

The first five eluting compounds (ETM, DMS, NPM, IPM and TBM) have very similar chemical structures and molecular weights; they elute at t=351, 386, 468, 581 and 653 s, respectively. This is highly conducive for in-field operations as analysis takes less than 11 minutes for these compounds, from sampling initiation to detection. Due to the high volatility of these mercaptans, a GC column with a strong sorbent coating was required to ensure separation. Ultimately, the DB-624 coating used in this platform's GC column was appropriate. ETM and DMS, the first two eluting compounds, have slight peak overlap. At 3 ppm, the resolution (R) as calculated was 2.4, above the commonly accepted 1.2 value to ensure adequate peak separation for quantification (t_2 and t_1 are retention times of DMS and ETM, respectively; w is peak width at half height).

Because THT has a heavier molecular weight and different structure than the other mercaptans, it elutes later at t=1317 s. Heating the GC column from 40 °C to 160 °C, as incorporated in the method, reduces the THT retention time than if the GC column were not heated, decreasing the total analysis time. For natural gas lines odorized with THT, the total analysis time is just under 22 minutes. There is work in the literature describing fast GC methods [67] that could be adapted

to reduce the analysis time; the hardware development required to implement such methods could be explored in future works.

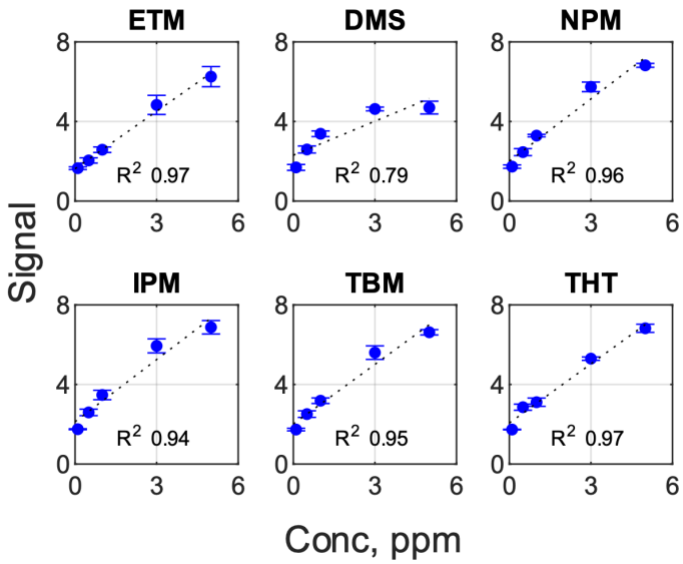

Figure 19. Calibration curves for six mercaptan analytes

The calibration data for each mercaptan are presented in **Figure 19**. A linear response was observed for mercaptans as concentrations increased. Five compounds had high R^2 values, which ranged from 0.94 to 0.97. Dimethyl sulfide had an R^2 value of 0.79, and future work will aim to improve the linear response of DMS.

The prediction model was based on a randomized 60% of calibration samples. Specifically, three samples were used to fit the calibration model and two samples were used for evaluating the prediction. The model parameters are summarized in **Table 4**. The platform's reproducibility for

Table 4. Linear calibration model parameters for predicting the mercaptan concentration in the samples

Compound	Slope	Y-axis	R-squared
ETM	1.03	-1.65	0.99
DMS	1.42	-2.9	0.81
NPM	0.92	-1.77	0.96
IPM	0.91	-1.83	0.94
TBM	0.96	-1.86	0.96
THT	0.98	-1.99	0.97

measured mercaptans (n=3): average relative standard deviation to measure a given mercaptan at a given concentration was 4.9%, with a median of 5.1% and a range of 0.8% - 10.0%.

After calibration of the instrument, the remaining randomized 40% of the data was used to validate its performance. Samples were generated by spiking Tedlar bags with known concentrations of mercaptans with nitrogen balance gas. **Figure 20** shows results for mercaptan concentration predictions against the actual mercaptan concentration of the sample. Higher error was observed for the lowest concentration, 0.1 ppm. This is likely due to the small signal generated by mercaptans at this concentration. Other factors could enhance detection of lower concentrations,

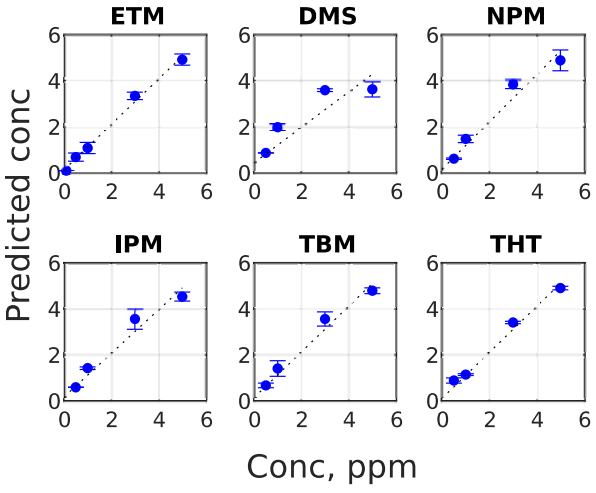

Figure 20. Predicted mercaptan concentrations

Predictions of mercaptan concentrations (conc) from a sample (y-axis) against the actual mercaptan concentration (x-axis).

such as increasing the sampling time; however, a target of 1 ppm was used herein. Excluding 0.1 ppm, the error observed ranged from 4.7 – 14.8% to accurately predict mercaptan concentrations. The intent of this platform is to monitor mercaptan levels to ensure their presence is above a certain concentration in distribution lines. Overall, the platform adequately predicted mercaptan concentrations in this proof-of-concept work. Future improvements to the platform will be considered to further decrease measurement variability. However, the platform as reported in this work can be deployed to monitor mercaptan levels in the concentration levels typically used in the industry.

We will further validate the platform under real world conditions, sampling natural gas from distribution lines and comparing our platform sensor readings against gold standard analytical measurements. This follow up work is ongoing, and we anticipate a subsequent publication forthcoming.

3.6 Conclusion

A portable chemical detection platform was developed and demonstrated for monitoring odorant compounds in natural gas. This platform provides the means to perform on-site odorant concentration monitoring from sample-to-analysis and is the first of its kind to our knowledge. Several odorant compounds were successfully separated and detected at concentrations commonly encountered in the field. This success of this work shows great promise in advancing gas phase chemical separation and sensing beyond the confines of the laboratory environment. Future work will explore opportunities to adapt this platform to perform on-site analysis of volatile organic compounds in other fields.

CHAPTER 4: Conclusions and Future Directions

In this chapter, dissertation findings and future directions for the work are summarized. Advancing gas phase chemical sensing portable platforms opens many opportunities for on-site field analysis of volatiles. In this work, we develop and demonstrate an ion detector to quantify concentrations of ionized VOCs. Then we integrate the detector system into a comprehensive platform to detect and quantify concentrations of natural gas odorants. This insight beyond the binary standard of human detection of odorization enables the separation and detection of specific odorant compounds such that the ratio of compound blends can be optimized.

4.1 Dissertation Findings

In this dissertation, a portable modular platform was developed to separate, detect, and quantify ionized gaseous VOCs. The detector was developed in-house to detect trace concentrations of ionized chemical compounds. Commercially available off the shelf components were utilized to construct much of the platform hardware such that this platform can be replicated and modified to meet the needs of future field research applications.

In Chapter 2, a low powered dual-polarity portable ion detector was developed and demonstrated to detect trace level chemicals. We developed the detector to investigate trace level ionized chemical detection with a microfabricated channel device. The custom electronics enable both manual and digital control of the ion sensing polarity mode while being powered off a low DC voltage and current draw. The physical device fixturing facilitates the entire nondestructive process from sample ionization to detection. The detector module achieves a small form factor suitable for standalone use and for adding detection capabilities to field equipment. The voltage output of the detector in both modes showed stable linear responses proportional to the chemical

concentrations tested. Detection capabilities down to 100 ppb were demonstrated for ion species of both positive and negative polarity.

In Chapter 3, the ion detector was integrated into a portable chemical detection platform subsequently developed and demonstrated for monitoring odorant compounds in natural gas. We developed this platform to investigate the separation and quantification of mercaptan compounds commonly used to odorize natural gas. This first of its kind platform provides the means to monitor odorant concentrations from sample-to-analysis. This platform was demonstrated successfully on a mixture of six commonly used mercaptan compounds (ethyl mercaptan, dimethyl sulfide, n-propylmercaptan, isopropyl mercaptan, tert-butyl mercaptan, and tetrahydrothiophene) at typical odorizing concentrations of 0.1 – 5 ppm. The success of this work shows great promise in advancing gas phase chemical separation and sensing beyond the confines of the laboratory environment.

4.2 Future Directions

4.2.1 Detector adding analysis dimension to other analytical techniques

Given the non-destructive nature of the ion detector, the sample from the detector outlet could be placed in-line with a downstream system that performs additional chemical analysis. The detector could offer initial information on the sample and studies could be performed with a mass spectrometer device in-tandem or following the detector. Similarly, the front end of the detector could be augmented to be downstream other analytical techniques such as IMS.

4.2.2 Platform extension to other applications

In this work, the platform was developed specifically for sensing natural gas odorants. The modularity of the platform allows for great potential for sensing other volatile compounds. Analysis components such as the sorbent trap and the GC column may be replaced or augmented to target other groups of volatile organic compounds.

4.2.3 Detection of metabolic volatiles

The core platform can be modified to detect metabolic volatiles such as food, plants, and breath samples. It is critical with such samples to collect, store, and transport with care given that the quality of such samples degrade over time. The platform developed in this work could be a significant step in bringing analysis on-site and closer to volatile samples, which in turn could reduce or outright eliminate the need for samples to be stored and transported. With breath

sample analysis, detection of volatiles can be used to diagnose health conditions. The platform components can be modified to be sensitive to target metabolic compounds.

4.2.4 Opportunities in platform development

The modular nature of the platform also translates to numerous research and development opportunities toward enabling on-site analysis of volatiles.

Ion source. The UV bulb was optimized for the odorant sensing application as the ionization energies matched those of mercaptan compounds. However, detection of negative ion yielding compounds, such as explosives, may require the integration of higher energy ionization sources like radioactive or corona discharge. This may present an opportunity to integrate a microfabricated device to retain the portable aspect of the platform as a whole or to shrink down both the size and power consumption.

Sample collection and introduction. The platform developed in this work facilitated samples to be either collected or to sample directly from natural gas lines. This portion of the platform generally will work well with collected samples. There are possibilities to innovate when moving to analysis of metabolic volatiles depending on the target applications. For example, the platform may be augmented to accept a microfabricated preconcentration device that combines sample collection and desorption into a single device. For on-site collection of human metabolites, the platform could be modified to collect human breath samples directly from subjects.

Component heating. The platform implements heating and temperature control with resistive heating elements and passive cooling. Investigation into more sophisticated control schemes and active cooling methods could yield better platform performance. Actively heated components

make up a large portion of the platform's energy requirements. Redirection of heat from components of the platform could lead to significant efficiency increases in power usage.

Appendix

Appendix A: Cleaning of Assembled Detector PCB Procedure

Materials:

- Scrubbing brush
- Ultrasonic bath (Branson 2800)
- Electronic cleaning formula for ultrasonic bath (Branson EC Solution)
- DI water
- Compressed air
- Drying oven (Optional)

1. Inspect the assembled PCB. Large contaminants can be initially removed physically with a scrubbing brush.
2. Prepare the electronic cleaning solution according to the formula manufacturer's instructions. (Branson EC 5% in DI water solution was used)

   WARNING: electronic cleaning solution is corrosive and must be handled carefully!
3. Outgas the solution by running the ultrasonic bath as instructed by the equipment manufacturer.
4. Submerge the PCB into the solution and run the ultrasonic bath for 10 minutes.
5. Transfer the PCB into DI water and run the ultrasonic bath for 10 minutes.
6. Inspect the PCB under a microscope to check for remaining contaminants (e.g., flux residues, foreign particles) especially near the input current path.
7. The cleaning steps may be repeated until the PCB is free of contaminants.
8. The PCB must be completely dried before use and this can be achieved with compressed air or placing into a drying oven.

Appendix B: Graphical User Interface (GUI) Tabs

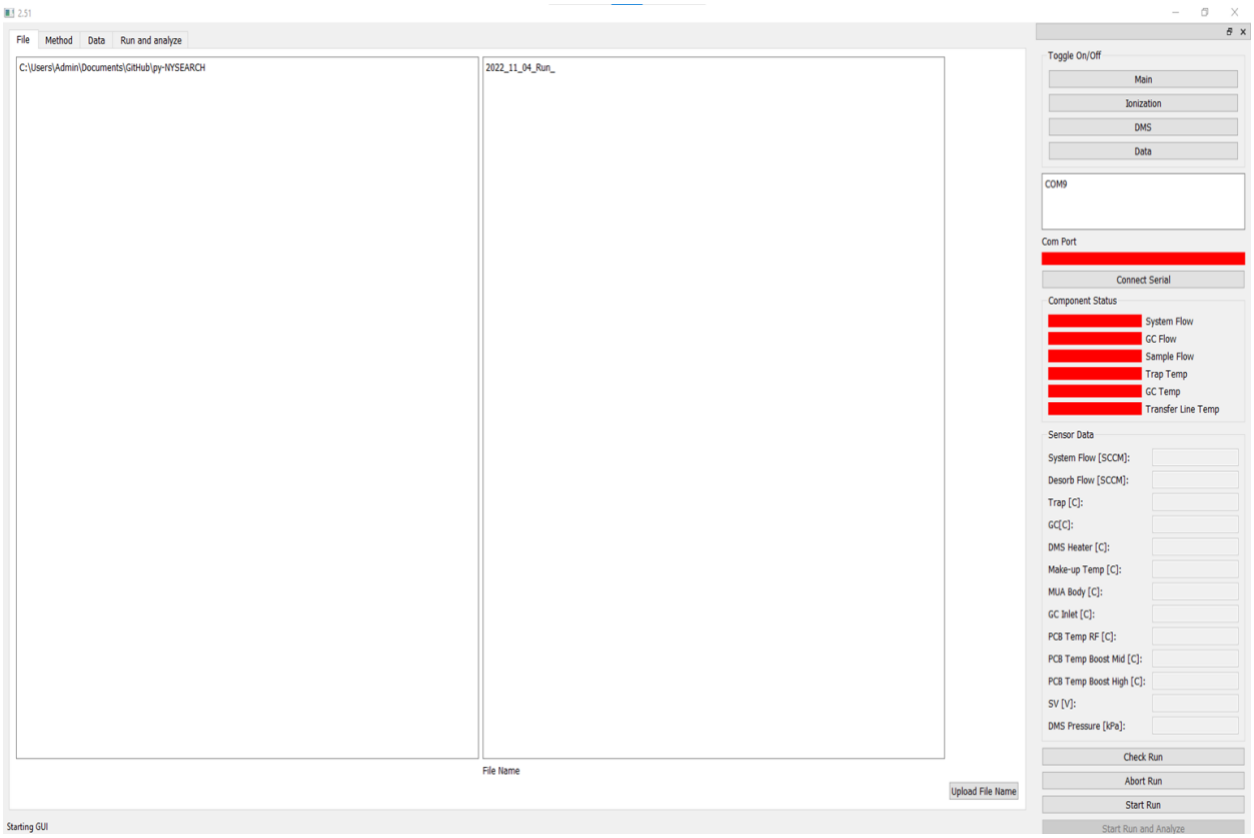

File Tab

This tab of the GUI is where the directory and the file name for data collected are set. The right sidebar facilitates device control and sensor readout, so it remains persistent throughout the program.

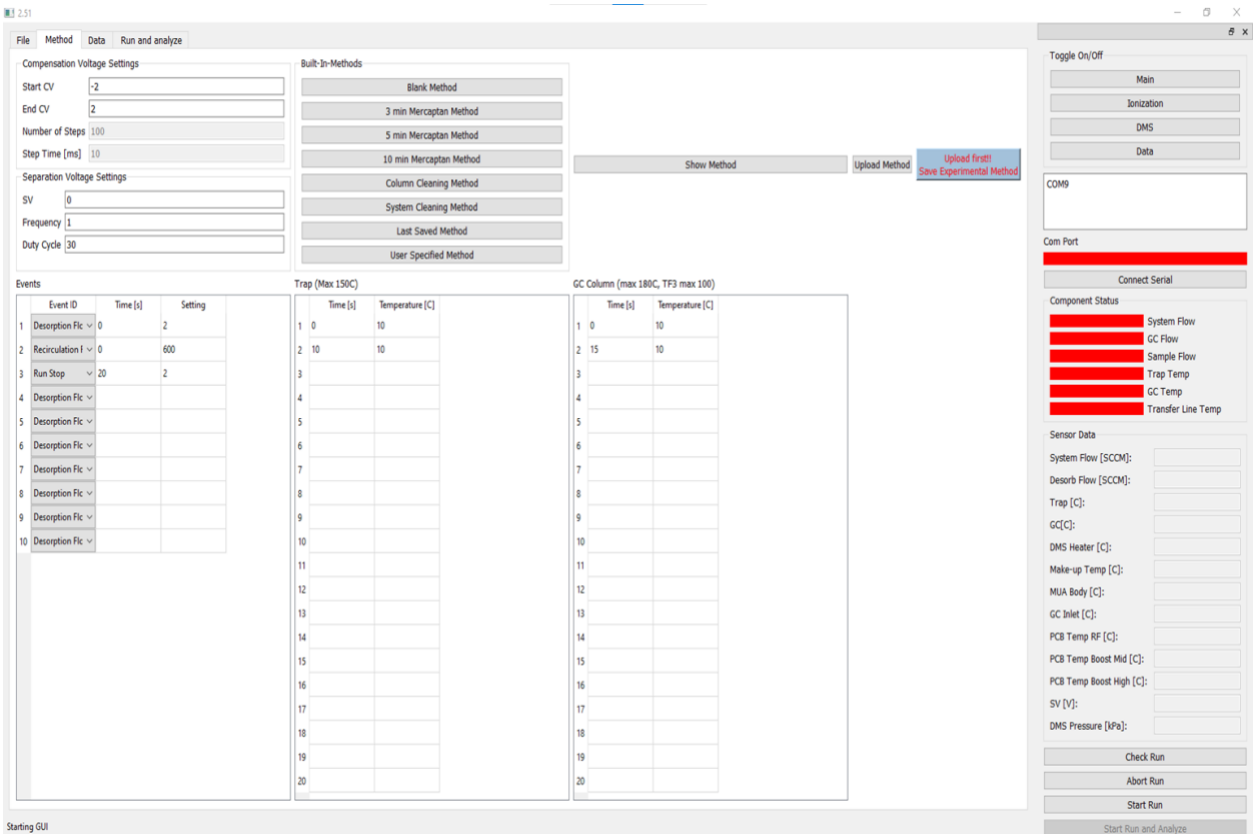

Method Tab

The method parameters are entered in this tab of the GUI. Waveform parameters are set in the top left. Flow control system commands are set under ‘Events’ while the temperature profiles for the trap and the GC column are set in their respective sections.

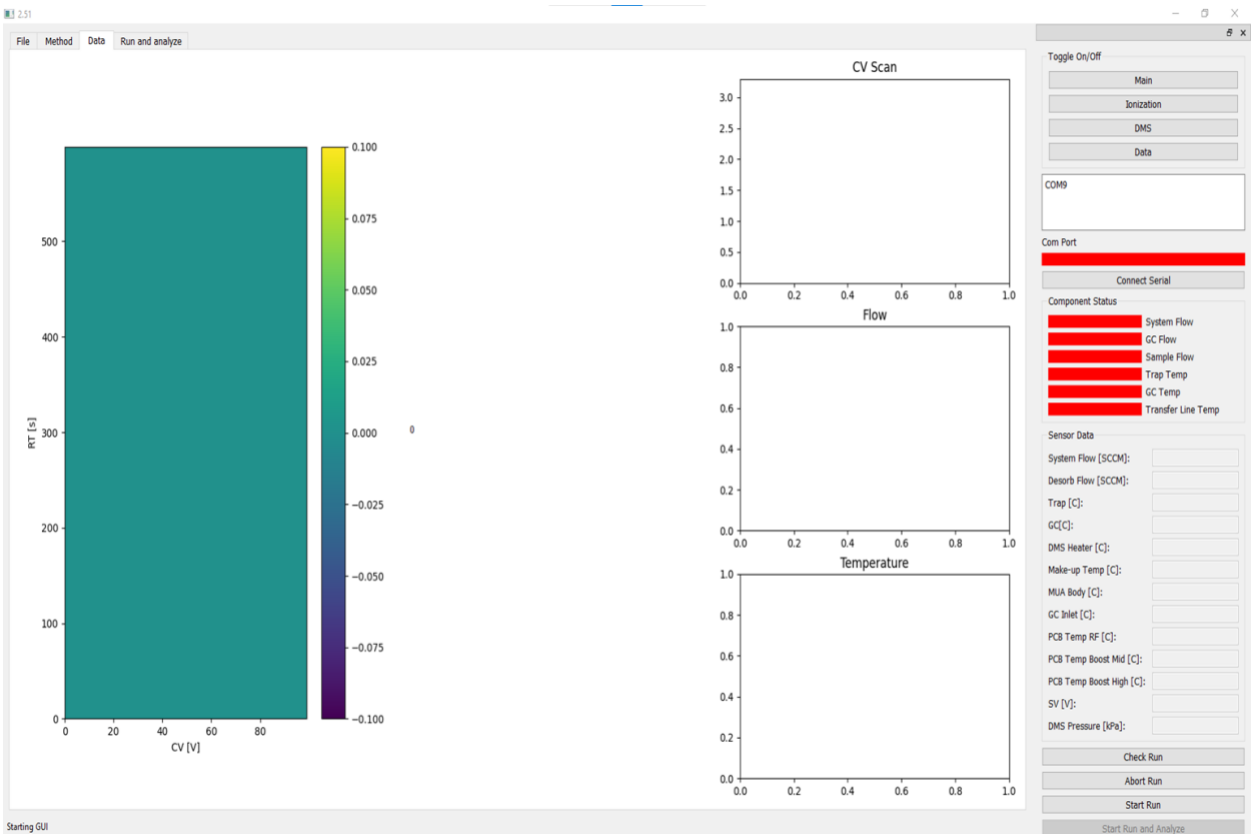

Data Tab

The Data Tab streams sensor data in real-time along with several other sensed parameters.

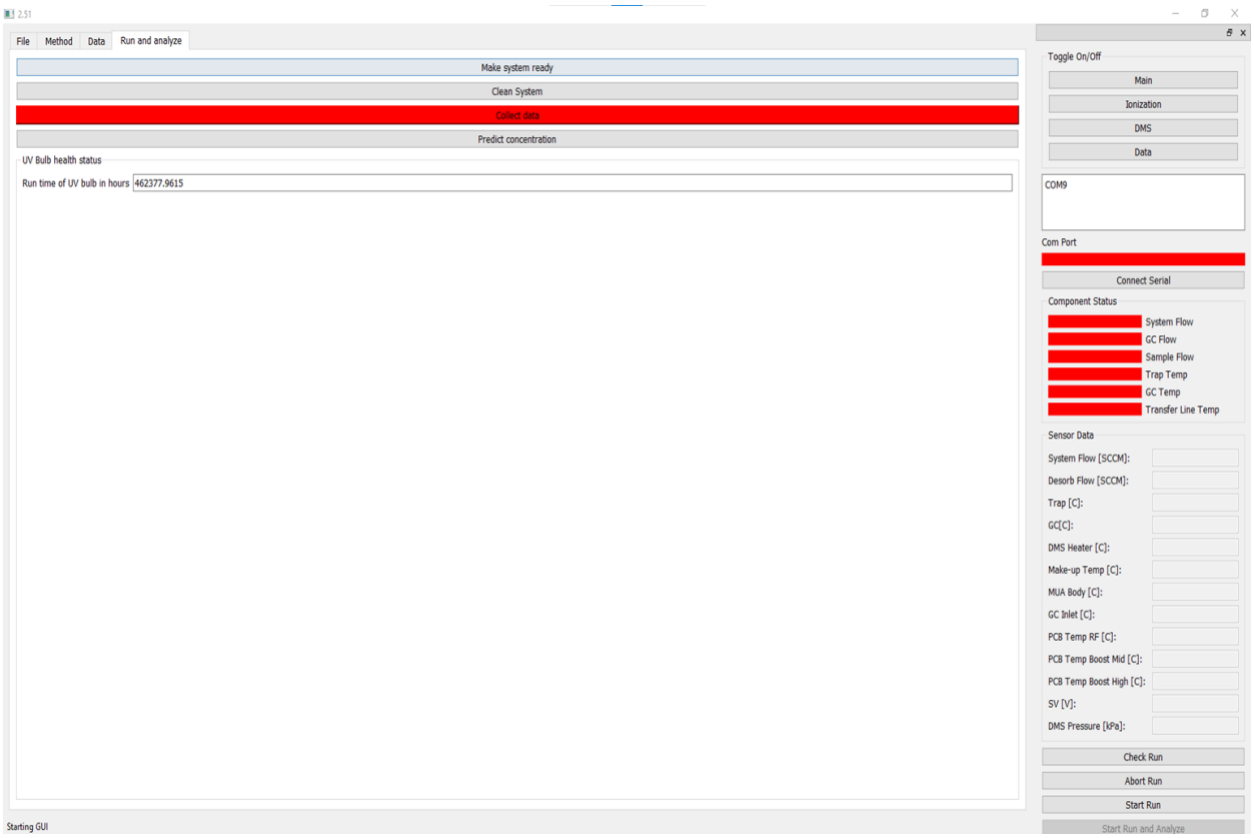

Run and Analyze Tab

This tab of the GUI is designed for minimally trained operator use. The ‘Collect data’ button automatically runs the method as described in the manuscript.

Appendix C: List of Materials

Part Number	Description	QTY	Vendor	Manufacturer
123-1334LTM	LTM GC column	1	Agilent	Agilent
NR1-3M-12	3-way isolation valve	3	Clippard	Clippard
D6F-01N2-000	Flow sensor	1	Digikey	Omron
HAFBLF0050CAAX5	Flow sensor	1	Digikey	Honeywell
HAFBLF0750C4AX5	Flow sensor	1	Digikey	Honeywell
MPXHZ6130A	Pressure sensor	1	Digikey	NXP/Freescale
NMP015	Sample pump	1	KNF	KNF
4406T12	10-32 O-ring seal to 1/8" ID barb	4	McMaster	N/A
5779K102	Push-to-Connect Tube Fitting for Air Straight Adapter, for 1/8" Tube OD x 1/8 NPT Male	2	McMaster	N/A
6763K81	Compresed air regulator	1	McMaster	N/A
98164A178	316 Stainless Steel Button Head Hex Drive Screw	130	McMaster	N/A
98164A119	Super-Corrosion-Resistant, 10-32 Thread Size, 1/2" Long	80	McMaster	N/A
3192T44	Routing Clamp Nylon Plastic, 1/2" ID, White, 1 [PCK] 18-8 Stainless Steel Washer for Number 6 Screw Size, 0.156" ID, 0.312" OD	6	McMaster	N/A
92949A833	18-8 Stainless Steel Button Head Hex Drive Screw 1/4"-20 Thread Size, 7/16" Long	8	McMaster	N/A
92673A113	18-8 Stainless Steel Hex Nut 1/4"-20 Thread Size, ASTM F594	4	McMaster	N/A
8560K219	Clear Scratch- and UV-Resistant Cast Acrylic Sheet 12" x 24" x 3/16"	4	McMaster	N/A
17715A75	Galvanized Steel Corner Bracket, 1.5" x 1.5" x 1.25"	31	McMaster	N/A
93505A197	Male-Female Threaded Hex Standoff Aluminum, 1/2" Hex Size, 1" Long, 1/4"-20 Thread Size	4	McMaster	N/A
97171A110	Brass Heat-Set Inserts for Plastic Flanged, 2-56 Thread Size, 0.157" Installed Length	80	McMaster	N/A
97171A130	Brass Heat-Set Inserts for Plastic Flanged, 6-32 Thread Size, 0.180" Installed Length	50	McMaster	N/A
92095A181	Button Head Hex Drive Screw Passivated 18-8 Stainless Steel, M3 x 0.50 mm Thread, 8mm Long	8	McMaster	N/A
92949A116	18-8 Stainless Steel Button Head Hex Drive Screw 1/4"-20 Thread Size, 7/16" Long	4	McMaster	N/A
7610N162	Push-to-Connect Tube Fitting, Stainless Steel, Straight, for 6mm OD, 1/4 Pipe Size	1	McMaster	N/A
DMS	Detector module	1	N/A	in-house
HL	Heated line assembly	3	N/A	in-house
Trap	Heated silica gel trap	1	N/A	in-house
17-216C-00-41+D3WFIL+BDO	Proportional valve	2	Norgren	Norgren/IMI
SS-2-TA-1-4RT	Male Tube Adapter, 1/4 in. Tube OD x 1/4 in. Male NPT	1	Swagelok	Swagelok
SS-200-1-0157	Male Connector, 1/8 in. Tube OD x #10-32 Male Thread	2	Swagelok	Swagelok
SS-200-3	Stainless Steel Tube Fitting, Union Tee, 1/8 in. Tube OD	1	Swagelok	Swagelok
SS-201-PC	Port Connector, 1/8 in. Tube OD	4	Swagelok	Swagelok
SS-SS2	Low Flow Metering Valve, 1/8 in. Swagelok Tube Fitting	2	Swagelok	Swagelok
EAOR21	10-32 O-ring seal to 1/8" external	4	Valco	Valco
EN2_ZF2-10	1/8 nut + ferrule	1	Valco	Valco
EZRU21	1/8" to 1/16" Ext/Int Reducing Union	1	Valco	Valco
FS.36-5	1/32" Valcon polyimide one-piece FS adapter 0.36 ≤ 0.40 mm	2	Valco	Valco
FS1.4-5	1/16" Valcon polyimide one-piece FS adapter 0.36 ≤ 0.40 mm	2	Valco	Valco
IZERA1.5M	1/16" to 1/32" internal to external reducer/adapter	1	Valco	Valco
MUA	Make-up Adapter	1	Valco	Valco
ZAOR11	O-ring to internal fitting adapter 10-32 to 1/16"	7	Valco	Valco
ZN1-10_ZF1-10	1/16" internal nut + ferrule	1	Valco	Valco
ZU1	1/16" internal union	1	Valco	Valco
ZUFR2	Filters for GC - Removable Screen	1	Valco	Valco

Appendix D: Electronics Circuit Schematics

Power Distribution Electronics

The device is mainly powered by a computer power supply via the ATX-24 connection from J1. From there, the various voltage levels are distributed to supply power to the rest of the platform electronic modules through cable harnesses. U2 is a DC-DC converter that provides a 24 V supply derived from the main supply's 12 V output. The LED (D1) provides visual confirmation that the main power supply has been switched on and is outputting power.

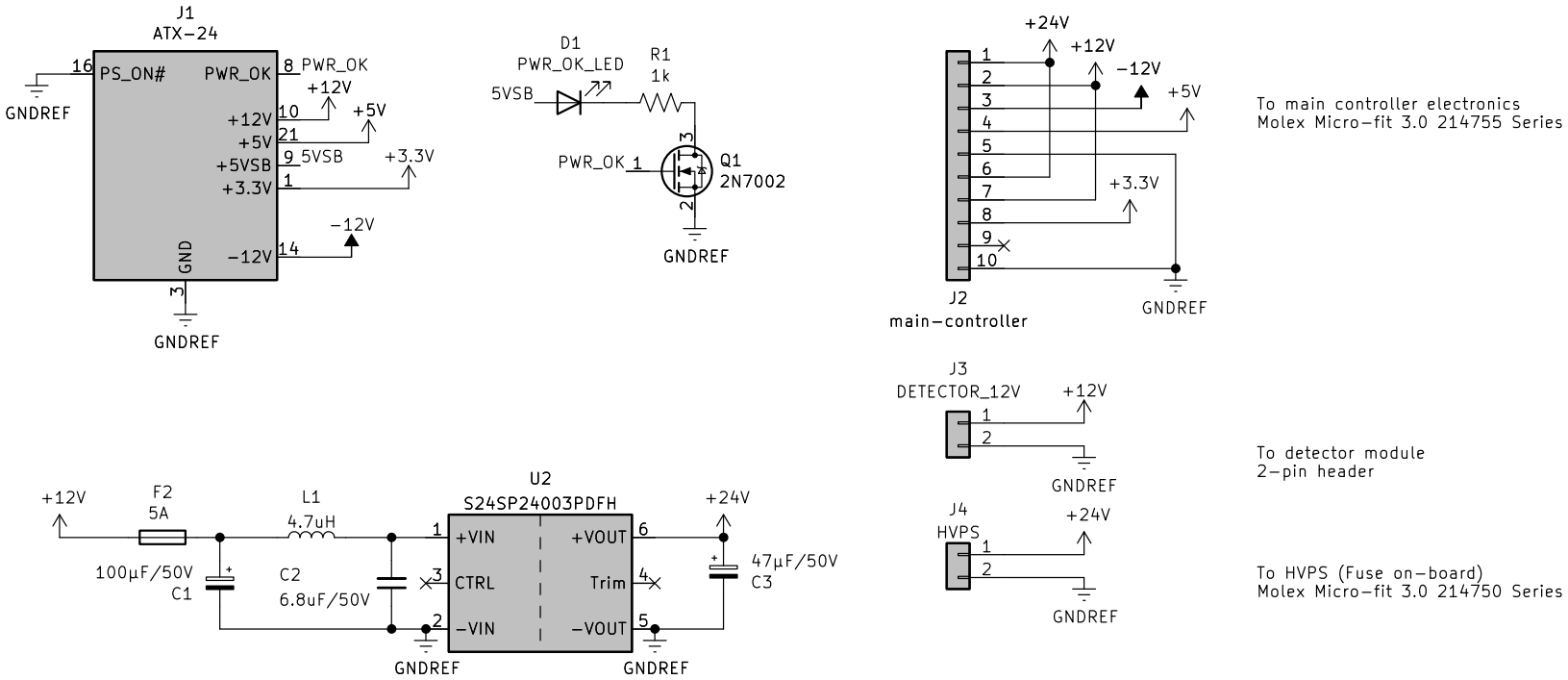

Power Distribution Electronics

High Voltage Power Supply (HVPS)

The HVPS powers the UV bulb ionization source for the detector. This circuit is powered by the same power source as the rest of the hardware but is electrically isolated by U1.

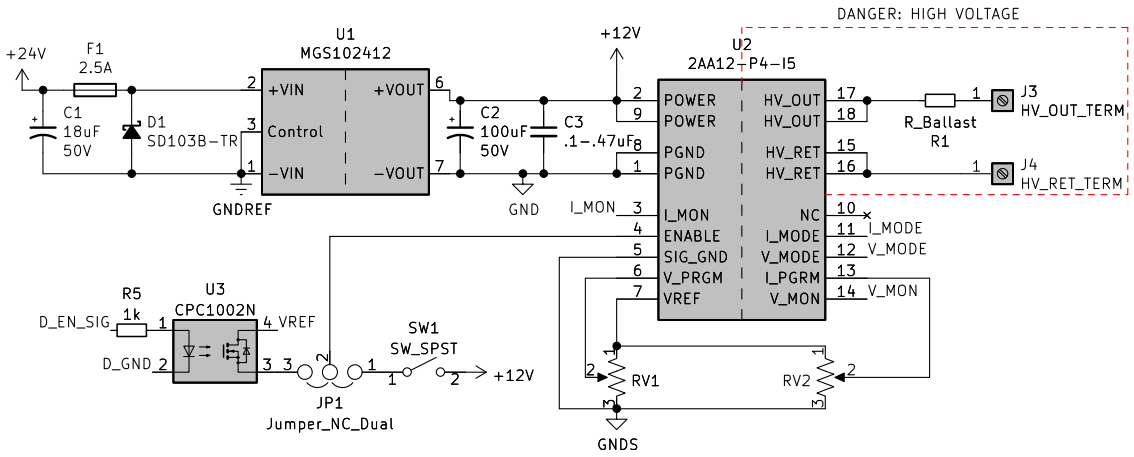

High Voltage Power Supply (HVPS)

Main Controller Electronics

The main controller printed circuit board (PCB) contains most of the platform electronics. The proportional valves are driven by a PWM signal that is digitally controlled by a DAC (digital to analog converter) IC. The signal from analog sensors is conditioned such that the signal voltage can be read by and do not damage the microcontroller pins. Two of the isolation valves are controlled with hit-and-hold circuits as recommended by the manufacturer. One of the isolation valves is only powered momentarily during each run and an inductive load driver is used. This same driver IC is used to drive the sample pump.

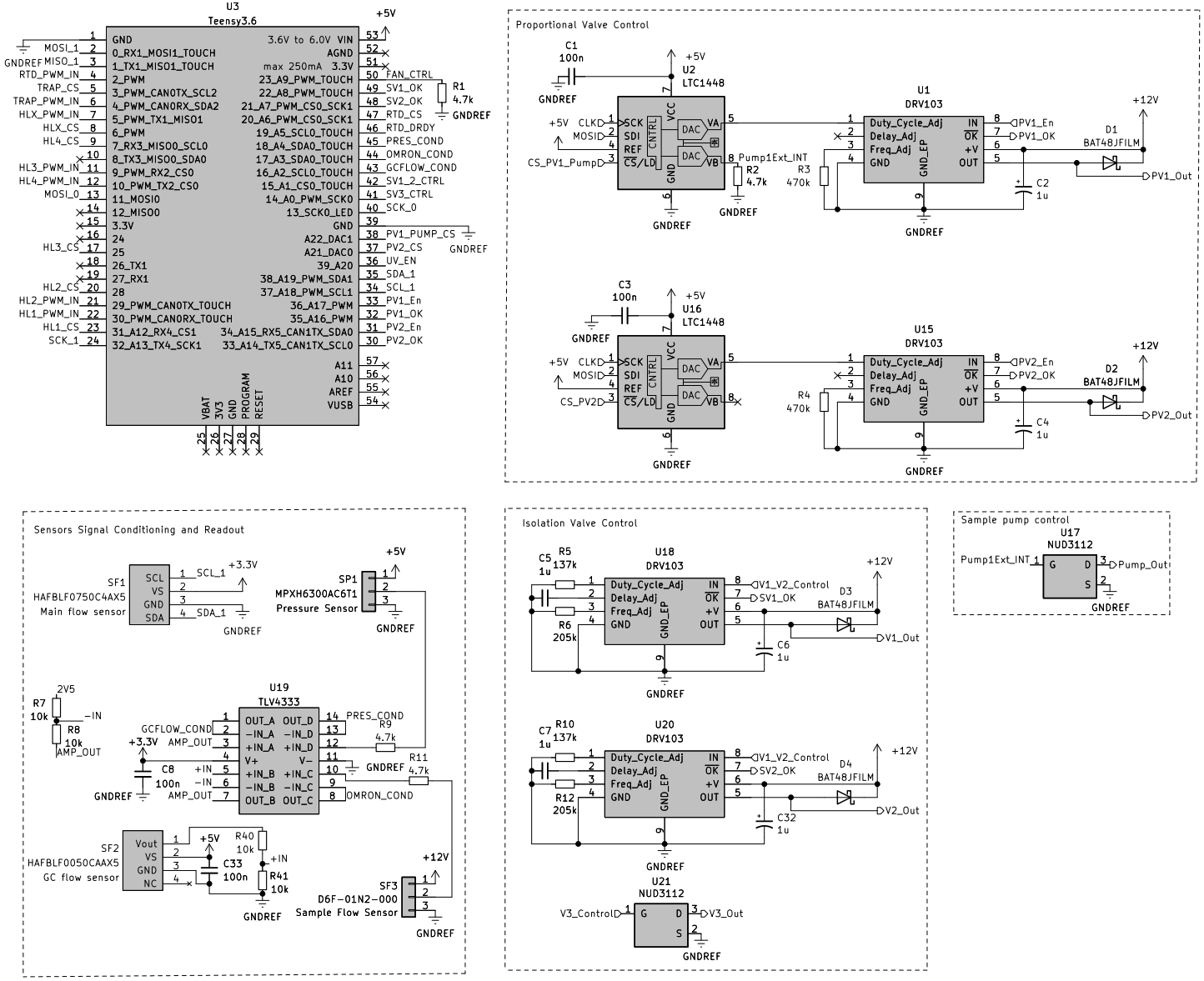

Main Controller Electronics

Heating Electronics

Each heated components is driven by PWM. The control is carried out in the microcontroller code that takes the respective temperature readings as an input. All heated devices, except for the GC column, have a thermocouple (TC) to sense temperature. Each TC is read by a cold-junction compensated thermocouple-to-digital converter IC. The GC column temperature is read by a resistive temperature detector (RTD). A precision analog-to-digital (ADC) IC package specified for precision sensor measurement was selected and configured to read the RTD.

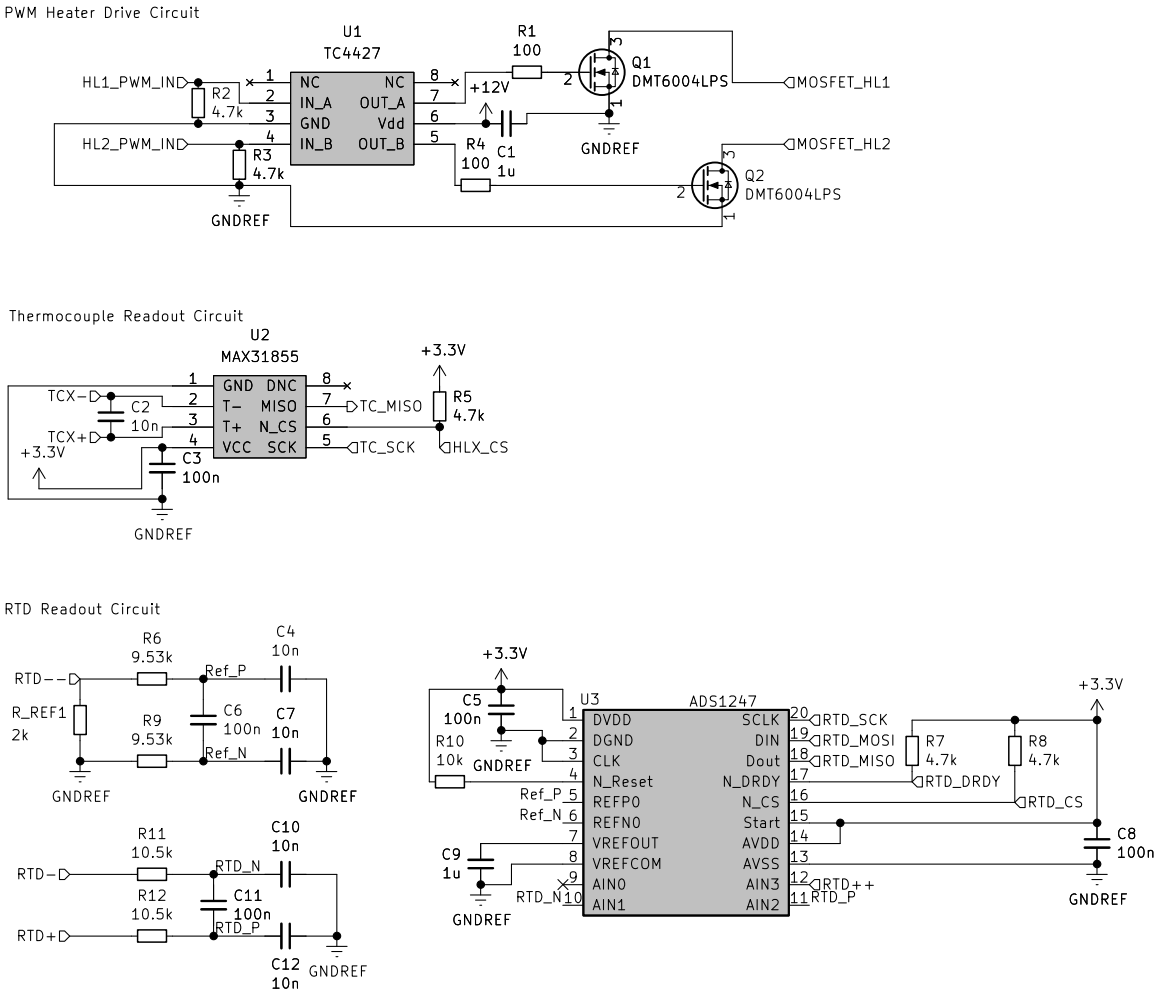

Heating Electronics

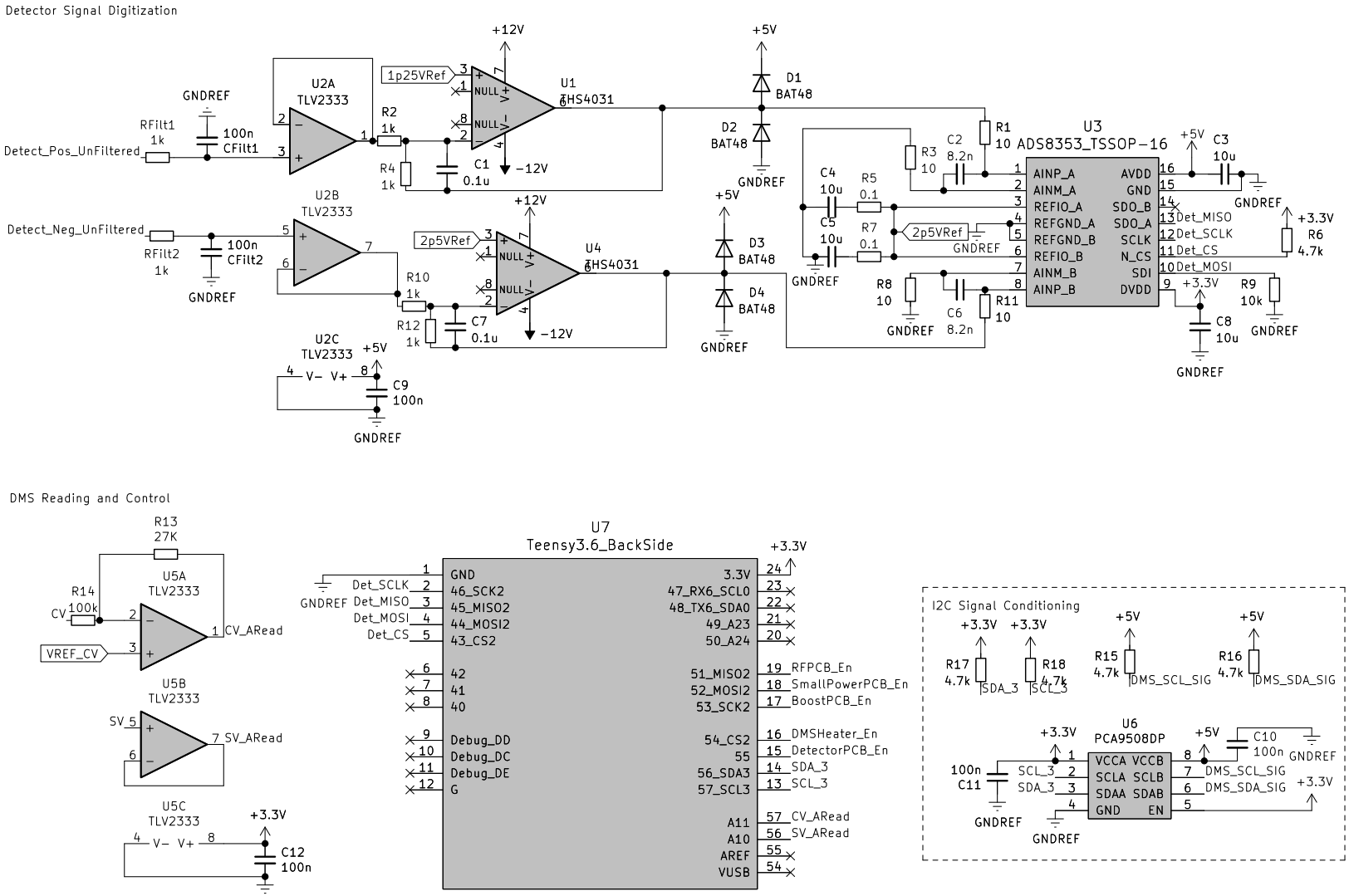

Detector Module Communications and Control (C&C) Electronics

Detector Module Communications and Control (C&C) Electronics

An auxiliary daughterboard was designed specifically to handle all the communications and control between the microcontroller and the detector module. A high-speed ADC package was selected to handle the detector signal output. Control of the detector module is accomplished with several digital outputs and I2C communications.

Appendix E: Heated Line Construction Procedure

Materials:

- Stainless steel tubing
- Tubing cutter
- Polyimide tube sleeving
- High temperature heat shrink tube sleeving
- K-type thermocouple
- Resistive (NiCr) heater wire
- Solder seal connectors

1. Measure and mark stainless steel tubing reserving enough extra tubing length for fittings on either side.	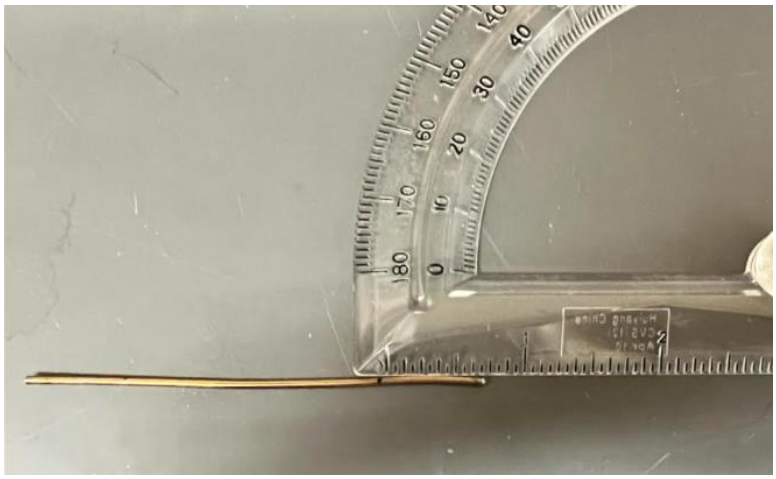
2. Cut the tubing to length. 1/16” tube cutter is shown.	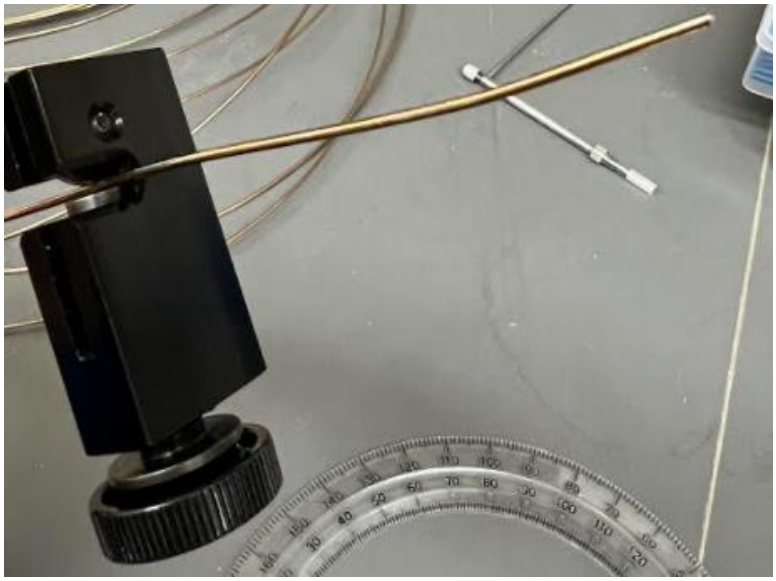

3. Measure and cut sleeving material reserving space at the ends for fittings. Slide the polyimide sleeving onto the tube.	
4. Slide the high temp heat shrink tubing with the thermocouple onto the polyimide sleeving. Position the thermocouple toward the middle of the heated line. Heat the heat shrink to secure the thermocouple and polyimide sleeve.	
5. Measure length of resistive heating wire to meet the desired resistance value or other characteristics. Coil the heating wire evenly onto the heat shrink layer.	

6. Finally, slide on another layer of high temperature heat shrink sleeving to protect, insulate, and secure the resistive heating wire coil. Electrical connections to the heating wire can be made using solder seal connectors.	

Appendix F: Temperature and Flow Data

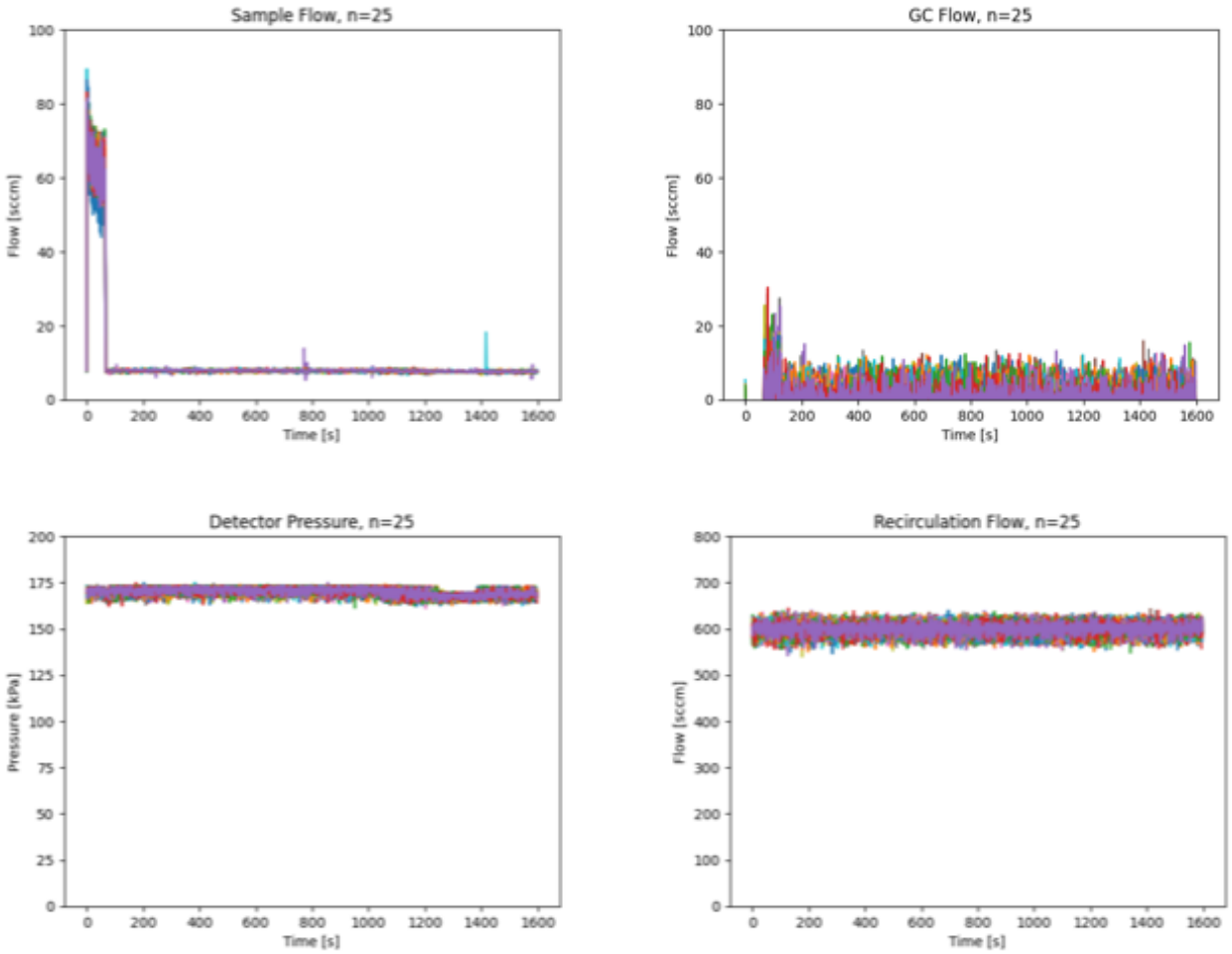

Flow and Pressure Data

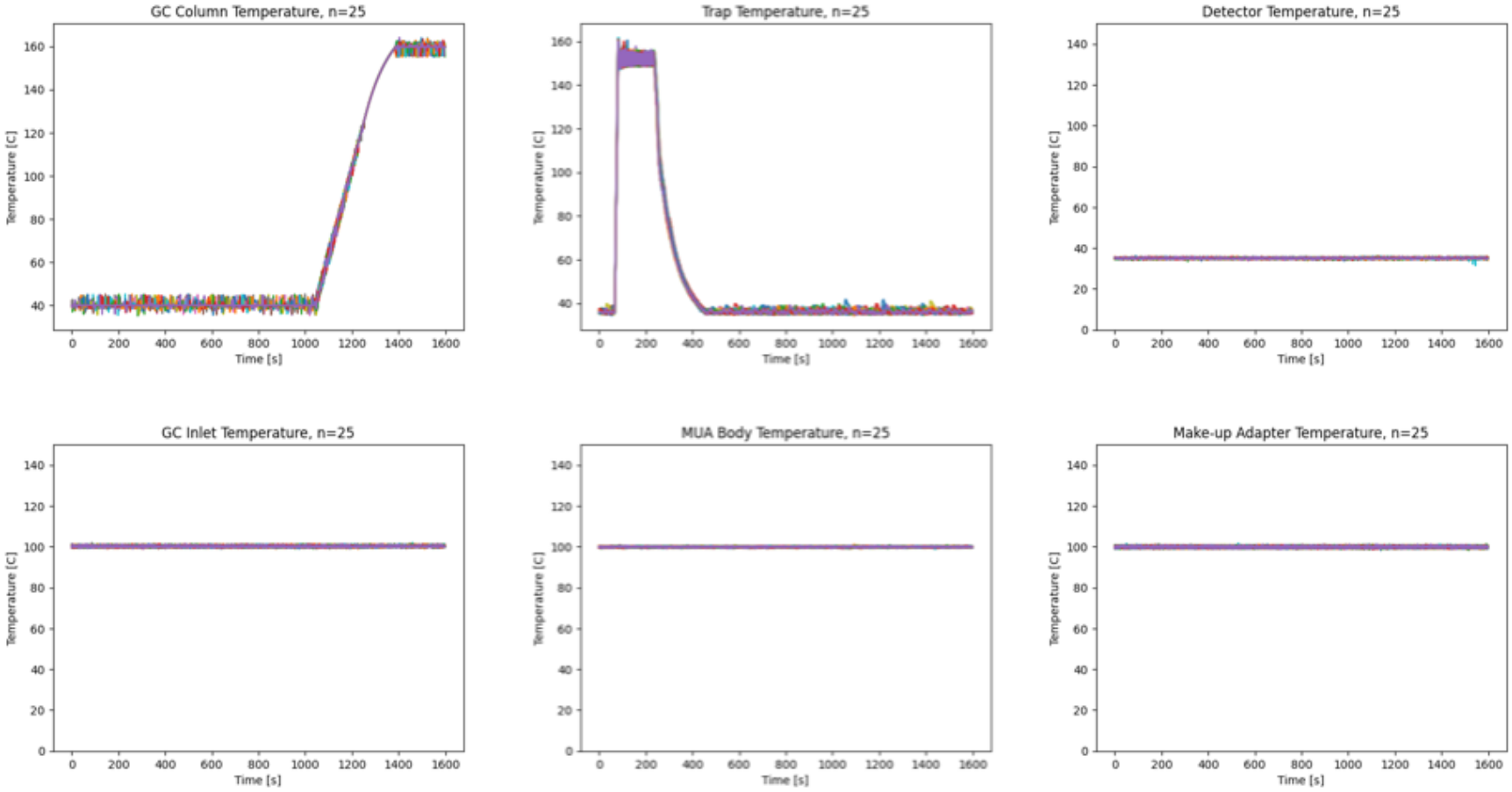

Temperature Data for Heated Device

References

[1] D. R. Gentner *et al.*, “Review of Urban Secondary Organic Aerosol Formation from Gasoline and Diesel Motor Vehicle Emissions,” *Environ Sci Technol*, vol. 51, no. 3, pp. 1074–1093, Feb. 2017, doi: 10.1021/acs.est.6b04509.

[2] B. C. McDonald *et al.*, “Volatile chemical products emerging as largest petrochemical source of urban organic emissions,” *Science (1979)*, vol. 359, no. 6377, pp. 760–764, Feb. 2018, doi: 10.1126/science.aaq0524.

[3] M. M. Rahman and K.-H. Kim, “Potential hazard of volatile organic compounds contained in household spray products,” *Atmos Environ*, vol. 85, pp. 266–274, Mar. 2014, doi: 10.1016/j.atmosenv.2013.12.001.

[4] U. B. Nurmatov, N. Tagieva, S. Semple, G. Devereux, and A. Sheikh, “Volatile organic compounds and risk of asthma and allergy: a systematic review and meta-analysis of observational and interventional studies,” *Primary Care Respiratory Journal 2013 22:1*, vol. 22, no. 1, pp. S9–S15, Mar. 2013, doi: 10.4104/pcrj.2013.00010.

[5] M. M. Elmassry and M. A. Farag, “In Vivo and In Vitro Volatile Organic Compounds (VOCs) Analysis in Bacterial Diagnostics: Case Studies in Agriculture and Human Diseases,” *Bacterial Volatile Compounds as Mediators of Airborne Interactions*, pp. 123–138, 2020, doi: 10.1007/978-981-15-7293-7_4.

[6] A. Pasamontes *et al.*, “Citrus tristeza virus infection in sweet orange trees and a mandarin × tangor cross alters low molecular weight metabolites assessed using gas chromatography mass spectrometry (GC/MS),” *Metabolomics 2016 12:3*, vol. 12, no. 3, pp. 1–10, Feb. 2016, doi: 10.1007/S11306-016-0959-Z.

[7] W. H. K. Cheung *et al.*, “Volatile organic compound (VOC) profiling of citrus tristeza virus infection in sweet orange citrus varietals using thermal desorption gas chromatography time of flight mass spectrometry (TD-GC/TOF-MS),” *Metabolomics 2015 11:6*, vol. 11, no. 6, pp. 1514–1525, May 2015, doi: 10.1007/S11306-015-0807-6.

[8] C. H. Thompson *et al.*, “Analysis of Volatile Profiles for Tracking Asymptomatic Infections of *Phytophthora ramorum* and other pathogens in *Rhododendron*,” *Phytopathology*, p. PHYTO-10-20-0472-R, Feb. 2021, doi: 10.1094/PHYTO-10-20-0472-R.

[9] M. M. McCartney *et al.*, “Effects of Phytophthora ramorum on volatile organic compound emissions of Rhododendron using gas chromatography–mass spectrometry,” *Analytical and Bioanalytical Chemistry 2017 410:5*, vol. 410, no. 5, pp. 1475–1487, Dec. 2017, doi: 10.1007/S00216-017-0789-5.

[10] R. M. C. Jansen *et al.*, “Health monitoring of plants by their emitted volatiles: A model to predict the effect of Botrytis cinerea on the concentration of volatiles in a large-scale

greenhouse," *Biosyst Eng*, vol. 106, no. 1, pp. 37–47, May 2010, doi: 10.1016/j.biosystemseng.2010.01.009.

[11] A. A. Aksenov *et al.*, "Metabolite Content Profiling of Bottlenose Dolphin Exhaled Breath," *Anal Chem*, vol. 86, no. 21, pp. 10616–10624, Nov. 2014, doi: 10.1021/ac5024217.

[12] R. Cumeras, W. H. K. Cheung, F. Gulland, D. Goley, and C. E. Davis, "Chemical Analysis of Whale Breath Volatiles: A Case Study for Non-Invasive Field Health Diagnostics of Marine Mammals," *Metabolites 2014, Vol. 4, Pages 790-806*, vol. 4, no. 3, pp. 790–806, Sep. 2014, doi: 10.3390/METABO4030790.

[13] A. T. Güntner, S. Abegg, K. Königstein, P. A. Gerber, A. Schmidt-Trucksäss, and S. E. Pratsinis, "Breath Sensors for Health Monitoring," *ACS Sens*, vol. 4, no. 2, pp. 268–280, Feb. 2019, doi: 10.1021/ACSSENSORS.8B00937.

[14] O. A. M. Popoola *et al.*, "Use of networks of low cost air quality sensors to quantify air quality in urban settings," *Atmos Environ*, vol. 194, pp. 58–70, Dec. 2018, doi: 10.1016/j.atmosenv.2018.09.030.

[15] A. J. Caban-Martinez *et al.*, "The 'Warm Zone' Cases: Environmental Monitoring Immediately Outside the Fire Incident Response Arena by Firefighters," *Saf Health Work*, vol. 9, no. 3, pp. 352–355, Sep. 2018, doi: 10.1016/j.shaw.2017.12.003.

[16] A. Gałuszka, Z. M. Migaszewski, and J. Namieśnik, "Moving your laboratories to the field – Advantages and limitations of the use of field portable instruments in environmental sample analysis," *Environ Res*, vol. 140, pp. 593–603, Jul. 2015, doi: 10.1016/j.envres.2015.05.017.

[17] L. T. Hagemann, M. M. McCartney, A. G. Fung, D. J. Peirano, C. E. Davis, and B. Mizaikoff, "Portable combination of Fourier transform infrared spectroscopy and differential mobility spectrometry for advanced vapor phase analysis," *Analyst*, vol. 143, no. 23, pp. 5683–5691, Nov. 2018, doi: 10.1039/C8AN01192C.

[18] I. M. Anishchenko *et al.*, "Modular and reconfigurable gas chromatography/differential mobility spectrometry (GC/DMS) package for detection of volatile organic compounds (VOCs)," *International Journal for Ion Mobility Spectrometry*, vol. 21, no. 4, pp. 125–136, Dec. 2018, doi: 10.1007/s12127-018-0240-4.

[19] M. Y. Rajapakse *et al.*, "An environmental air sampler to evaluate personal exposure to volatile organic compounds," *Analyst*, vol. 146, no. 2, pp. 636–645, 2021, doi: 10.1039/D0AN01521K.

[20] A. G. Fung *et al.*, "Wearable Environmental Monitor To Quantify Personal Ambient Volatile Organic Compound Exposures," *ACS Sens*, vol. 4, no. 5, pp. 1358–1364, May 2019, doi: 10.1021/acssensors.9b00304.

[21] M. M. McCartney *et al.*, “An Easy to Manufacture Micro Gas Preconcentrator for Chemical Sensing Applications,” *ACS Sens*, vol. 2, no. 8, pp. 1167–1174, Aug. 2017, doi: 10.1021/acssensors.7b00289.

[22] N. Strand, A. Bhushan, M. Schivo, N. J. Kenyon, and C. E. Davis, “Chemically polymerized polypyrrole for on-chip concentration of volatile breath metabolites,” *Sens Actuators B Chem*, vol. 143, no. 2, pp. 516–523, Jan. 2010, doi: 10.1016/j.snb.2009.09.052.

[23] S. Zampolli, I. Elmi, G. C. Cardinali, L. Masini, F. Bonafè, and F. Zardi, “Compact-GC platform: A flexible system integration strategy for a completely microsystems-based gas-chromatograph,” *Sens Actuators B Chem*, vol. 305, no. November 2019, p. 127444, Feb. 2020, doi: 10.1016/j.snb.2019.127444.

[24] R. R. A. Syms and S. Wright, “MEMS mass spectrometers: the next wave of miniaturization,” *Journal of Micromechanics and Microengineering*, vol. 26, no. 2, p. 023001, Feb. 2016, doi: 10.1088/0960-1317/26/2/023001.

[25] A. T. Kirk, M. Allers, P. Cochems, J. Langejuergen, and S. Zimmermann, “A compact high resolution ion mobility spectrometer for fast trace gas analysis,” *Analyst*, vol. 138, no. 18, p. 5200, Sep. 2013, doi: 10.1039/c3an00231d.

[26] W. Wang *et al.*, “Rapid Screening of Trace Volatile and Nonvolatile Illegal Drugs by Miniature Ion Trap Mass Spectrometry: Synchronized Flash-Thermal-Desorption Purging and Ion Injection,” *Anal Chem*, vol. 91, no. 15, pp. 10212–10220, Aug. 2019, doi: 10.1021/acs.analchem.9b02309.

[27] M. Wei-Hao Li, A. Ghosh, A. Venkatasubramanian, R. Sharma, X. Huang, and X. Fan, “High-Sensitivity Micro-Gas Chromatograph–Photoionization Detector for Trace Vapor Detection,” *ACS Sens*, vol. 6, no. 6, pp. 2348–2355, Jun. 2021, doi: 10.1021/acssensors.1c00482.

[28] G. A. Eiceman *et al.*, “Miniature radio-frequency mobility analyzer as a gas chromatographic detector for oxygen-containing volatile organic compounds, pheromones and other insect attractants,” *J Chromatogr A*, vol. 917, no. 1–2, pp. 205–217, May 2001, doi: 10.1016/S0021-9673(01)00656-2.

[29] S. K. Guharay, P. Dwivedi, and H. H. Hill, “Ion Mobility Spectrometry: Ion Source Development and Applications in Physical and Biological Sciences,” *IEEE Transactions on Plasma Science*, vol. 36, no. 4, pp. 1458–1470, Aug. 2008, doi: 10.1109/TPS.2008.927290.

[30] F. Gunzer, A. Ulrich, and W. Baether, “A novel non-radioactive electron source for ion mobility spectrometry,” *International Journal for Ion Mobility Spectrometry*, vol. 13, no. 1, pp. 9–16, Mar. 2010, doi: 10.1007/s12127-009-0034-9.

[31] P. Cochems, M. Runge, and S. Zimmermann, “A current controlled miniaturized non-radioactive electron emitter for atmospheric pressure chemical ionization based on thermionic emission,” *Sens Actuators A Phys*, vol. 206, pp. 165–170, Feb. 2014, doi: 10.1016/j.sna.2013.11.033.

[32] G. Coelho Rezende, S. Le Calvé, J. J. Brandner, and D. Newport, “Micro photoionization detectors,” *Sens Actuators B Chem*, vol. 287, no. February, pp. 86–94, May 2019, doi: 10.1016/j.snb.2019.01.072.

[33] S. Evans, “[3] Detectors,” in *Methods in Enzymology*, vol. 193, no. C, Academic Press, 1990, pp. 61–86. doi: 10.1016/0076-6879(90)93411-D.

[34] Agilent Technologies, “Agilent 5977 Series MSD System Concepts Guide.” Accessed: Aug. 24, 2023. [Online]. Available: https://www.agilent.com/cs/library/usermanuals/public/user-manual-msd-system-5977-concept-guide-G7077-90036-en-agilent.pdf

[35] G. A. Eiceman, Z. Karpas, and H. H. Hill Jr., *Ion Mobility Spectrometry*. CRC Press, 2013. doi: 10.1201/b16109.

[36] M. McKeown, “Instrumentation for negative ion detection.,” *Environ Health Perspect*, vol. 36, pp. 97–101, Jun. 1980, Accessed: Jun. 24, 2018. [Online]. Available: http://www.ncbi.nlm.nih.gov/pubmed/7428750

[37] M. He, P. Marzocca, and S. Dhaniyala, “A new high performance battery-operated electrometer,” *Review of Scientific Instruments*, vol. 78, no. 10, p. 105103, Oct. 2007, doi: 10.1063/1.2789659.

[38] S. Weigl, F. Feldmeier, R. Bierl, and F.-M. Matysik, “Photoacoustic detection of acetone in N2 and synthetic air using a high power UV LED,” *Sens Actuators B Chem*, vol. 316, p. 128109, Aug. 2020, doi: 10.1016/j.snb.2020.128109.

[39] S. Narayanan, G. Rice, and M. Agah, “A micro-discharge photoionization detector for micro-gas chromatography,” *Microchimica Acta*, vol. 181, no. 5–6, pp. 493–499, Apr. 2014, doi: 10.1007/s00604-013-1146-9.

[40] P. Intra and N. Tippayawong, “Development and Evaluation of a Faraday Cup Electrometer for Measuring and Sampling Atmospheric Ions and Charged Aerosols,” *Particulate Science and Technology*, vol. 33, no. 3, pp. 257–263, May 2015, doi: 10.1080/02726351.2014.952392.

[41] S. O. Agbroko and J. Covington, “A novel, low-cost, portable PID sensor for the detection of volatile organic compounds,” *Sens Actuators B Chem*, vol. 275, pp. 10–15, Dec. 2018, doi: 10.1016/j.snb.2018.07.173.

[42] US Energy Information Administration, “U.S. energy consumption by source and sector, 2021,” Apr. 2022. Accessed: Oct. 13, 2022. [Online]. Available:

https://web.archive.org/web/20221104010524/https://www.eia.gov/totalenergy/data/monthly/pdf/flow/total-energy-spaghettichart-2021.pdf

[43] D. R. Michanowicz *et al.*, “Home is Where the Pipeline Ends: Characterization of Volatile Organic Compounds Present in Natural Gas at the Point of the Residential End User,” *Environmental Science & Technology*, vol. 56, no. 14, pp. 10258–10268, Jun. 2022, doi: 10.1021/acs.est.1c08298.

[44] S. Solomon *et al.*, “IPCC (2007). Climate Change 2007: The Physical Science Basis,” Cambridge, 2007. [Online]. Available: http://www.ipcc.ch/report/ar4/

[45] A. J. Kidnay, W. R. Parrish, and D. G. McCartney, *Fundamentals of Natural Gas Processing*. CRC Press, 2011. doi: 10.1201/b14397.

[46] Chevron Phillips Chemical, “Odor-Fade Warning.” Accessed: Feb. 25, 2023. [Online]. Available: https://web.archive.org/web/20230226205455/https://www.cpchem.com/odor-fade-warning

[47] S. Sironi, L. Capelli, K. Haerens, P. Segers, and T. Van Elst, “Sampling And Stability of Mercaptans: Comparison Between Bags, Canisters and Sorbent Tubes,” *Chem Eng Trans*, vol. 54, 2016, doi: 10.3303/CET1654006.

[48] A. de Angelis, “Natural gas removal of hydrogen sulphide and mercaptans,” *Appl Catal B*, vol. 113–114, pp. 37–42, Feb. 2012, doi: 10.1016/j.apcatb.2011.11.026.

[49] F. V. Wilby, “Variation in Recognition Odor Threshold of a Panel,” *J Air Pollut Control Assoc*, vol. 19, no. 2, pp. 96–100, Feb. 1969, doi: 10.1080/00022470.1969.10466466.

[50] A. M. Khan, D. Kallogjeri, and J. F. Piccirillo, “Growing Public Health Concern of COVID-19 Chronic Olfactory Dysfunction,” *JAMA Otolaryngology–Head & Neck Surgery*, vol. 148, no. 1, pp. 81–82, Jan. 2022, doi: 10.1001/JAMAOTO.2021.3379.

[51] Y. Zrodnikov, M. Y. Rajapakse, D. J. Peirano, A. A. Aksenov, N. J. Kenyon, and C. E. Davis, “High Asymmetric Longitudinal Field Ion Mobility Spectrometry Device for Low Power Mobile Chemical Separation and Detection,” *Anal Chem*, vol. 91, no. 9, pp. 5523–5529, May 2019, doi: 10.1021/acs.analchem.8b05577.

[52] R. B. Schulz, V. C. Plantz, and D. R. Brush, “Shielding Theory and Practice,” *IEEE Trans Electromagn Compat*, vol. 30, no. 3, pp. 187–201, 1988, doi: 10.1109/15.3297.

[53] C. Pochet, H. Jiang, and D. A. Hall, “Ultra-low leakage ESD protection achieving 10.5 FA leakage,” *Proceedings - IEEE International Symposium on Circuits and Systems*, vol. 2021-May, 2021, doi: 10.1109/ISCAS51556.2021.9401369.

[54] D. Yeap *et al.*, “Machine Vision Methods, Natural Language Processing, and Machine Learning Algorithms for Automated Dispersion Plot Analysis and Chemical Identification from Complex Mixtures,” *Anal Chem*, vol. 91, no. 16, pp. 10509–10517, Aug. 2019, doi: 10.1021/acs.analchem.9b01428.

[55] M. Y. Rajapakse, J. A. Stone, and G. A. Eiceman, “Decomposition Kinetics of Nitroglycerine·Cl–(g) in Air at Ambient Pressure with a Tandem Ion Mobility Spectrometer,” *J Phys Chem A*, vol. 118, no. 15, pp. 2683–2692, Apr. 2014, doi: 10.1021/jp412444b.

[56] S. Fung *et al.*, “Portable chemical detection platform for on-site monitoring of odorant levels in natural gas,” *J Chromatogr A*, p. 464151, Jun. 2023, doi: 10.1016/j.chroma.2023.464151.

[57] A. S. Brown *et al.*, “Sampling of gaseous sulfur-containing compounds at low concentrations with a review of best-practice methods for biogas and natural gas applications,” *TrAC Trends in Analytical Chemistry*, vol. 64, pp. 42–52, Jan. 2015, doi: 10.1016/J.TRAC.2014.08.012.

[58] J. Luong, R. Gras, R. Mustacich, and H. Cortes, “Low Thermal Mass Gas Chromatography: Principles and Applications,” *J Chromatogr Sci*, vol. 44, no. 5, pp. 253–261, May 2006, doi: 10.1093/CHROMSCI/44.5.253.

[59] R. A. Miller, G. A. Eiceman, E. G. Nazarov, and A. T. King, “A novel micromachined high-field asymmetric waveform-ion mobility spectrometer,” *Sens Actuators B Chem*, vol. 67, no. 3, pp. 300–306, Sep. 2000, doi: 10.1016/S0925-4005(00)00535-9.

[60] I. A. Buryakov, E. V. Krylov, E. G. Nazarov, and U. Kh. Rasulev, “A new method of separation of multi-atomic ions by mobility at atmospheric pressure using a high-frequency amplitude-asymmetric strong electric field,” *Int J Mass Spectrom Ion Process*, vol. 128, no. 3, pp. 143–148, Oct. 1993, doi: 10.1016/0168-1176(93)87062-W.

[61] S. Fung *et al.*, “Battery powered dual-polarity ion detector for trace chemical sensing,” *Sens Actuators A Phys*, vol. 338, p. 113442, May 2022, doi: 10.1016/j.sna.2022.113442.

[62] B. Smith Barry, “Overview Of Flashlamps And Arc Lamps,” *https://doi.org/10.1117/12.966620*, vol. 0609, no. 30, pp. 1–41, Jun. 1986, doi: 10.1117/12.966620.

[63] D. J. Peirano, A. Pasamontes, and C. E. Davis, “Supervised semi-automated data analysis software for gas chromatography / differential mobility spectrometry (GC/DMS) metabolomics applications,” *International Journal for Ion Mobility Spectrometry*, vol. 19, no. 2–3, pp. 155–166, Sep. 2016, doi: 10.1007/s12127-016-0200-9.

[64] D. Yeap, M. M. McCartney, M. Y. Rajapakse, A. G. Fung, N. J. Kenyon, and C. E. Davis, “Peak detection and random forests classification software for gas chromatography/differential mobility spectrometry (GC/DMS) data,” *Chemometrics and Intelligent Laboratory Systems*, vol. 203, p. 104085, Aug. 2020, doi: 10.1016/j.chemolab.2020.104085.

[65] P. Chakraborty, M. Y. Rajapakse, M. M. McCartney, N. J. Kenyon, and C. E. Davis, “Machine learning and signal processing assisted differential mobility spectrometry (DMS)

data analysis for chemical identification," *Analytical Methods*, vol. 14, no. 34, pp. 3315–3322, Sep. 2022, doi: 10.1039/D2AY00723A.

[66] M. Y. Rajapakse, E. Borras, D. Yeap, D. J. Peirano, N. J. Kenyon, and C. E. Davis, "Automated chemical identification and library building using dispersion plots for differential mobility spectrometry," *Analytical Methods*, vol. 10, no. 35, pp. 4339–4349, Sep. 2018, doi: 10.1039/C8AY00846A.

[67] M. Zoccali, P. Q. Tranchida, and L. Mondello, "Fast gas chromatography-mass spectrometry: A review of the last decade," *TrAC Trends in Analytical Chemistry*, vol. 118, pp. 444–452, Sep. 2019, doi: 10.1016/j.trac.2019.06.006.